CHARACTERIZATION OF GPR139 AND INVESTIGATING ITS POSSIBLE ROLE IN BRAIN DEVELOPMENT

by

Tolga Aslan

B.S., Molecular Biology and Genetics, Boğaziçi University, 2006

M.S., Molecular Biology and Genetics, Boğaziçi University, 2009

Submitted to the Institute for Graduate Studies in
Science and Engineering in partial fulfillment of
the requirements for the degree of
Doctor of Philosophy

Graduate Program in Molecular Biology and Genetics

Boğaziçi University

2022

To my family...

ACKNOWLEDGEMENTS

I would like to thank my supervisor Assist. Prof. Necla Birgül for her valuable criticism, teaching me critical thinking and how to approach problems I have encountered during my studies.

I would like to thank my committee members for spending their valuable time in evaluating and criticizing this work.

I would also like to thank the academic members of our department for teaching me to become a better scientist and person.

I sincerely believe it would be much harder and much less-entertaining journey without the current and former members of our laboratory. I would like to thank Tuncay Şeker, Ph.D., İzzet Akiva, Ph.D., Aida Shahraki, Ph.D., Burçin Duan Şahbaz, Ph.D., Gökhan Gür, Ph.D., Barbaros Düzgün, Ali İşbilir, Ph.D. and all special project students who joined NBI-CSL lab for their help and friendship.

I have a long list of friends in the department to thank. The people I bothered the most deserve special thanks: Mehmet Can Demirler, Ph.D., Yiğit Kocagöz, Ph.D, H. Ayşin Akpınar, Ph.D., and Gizem Gül. I probably have picked a lot of people's brains in the department with a couple of questions so in short, I would like to express my gratitude to anyone helped me through my studies in any way.

I also would like to thank Erşen Kavak, Ph.D, for teaching me the ways of bioinformatics and enabling me to add valuable analyses to this study and for his friendship.

Major part of animal experiments was done in İstanbul and Medipol Universities. I would like to thank Prof. Serhat Papuccuoğlu, Prof. Sema Birler, Prof. Kamber Demir, Andaç Kılıçkap and the staff at İstanbul University Faculty of Veterinary Sciences Department of Reproduction and Artificial Insemination.

I am also grateful to Assist. Prof. Deniz Atasoy and Pelin Dilsiz, Ph.D. for their help and insight in *in vivo* ablation experiments, Assist. Prof. Muhammed İkbal Alp and Rümeysa A. for their help in final stages of my experiments. I also would like to thank Prof. Gürkan Öztürk and the REMER staff for helping my during my studies. I thank my friends in Vivarium who made the time I spent with animals much more bearable and provided me with their friendship and help.

I am also grateful to thank my family for their endless love, support and understanding and making me the person who I am today.

Lastly I would like to express my heartfelt gratitude to two most important people in my life: my wife Şenay Cengiz Aslan and my beloved son Erkin Bilge Aslan. If it weren't for Şenay, I wouldn't be able to write these lines today. She helped me through my darkest hours and for that, I am forever grateful. Erkin was born during the first years of my doctoral studies and brought joy and meaning to my life. Without his hugs, kisses, and smiles, I wouldn't be able to gather my strength to go on. They have always been the wind in my sails, supporting me when I needed the most. I am thankful to them both for their support but most importantly for the unconditional love they shared with me.

The work presented here was partly supported by Boğaziçi University Scientific Research Projects (project codes: 18B01D3 and 20B01D2).

ABSTRACT

CHARACTERIZATION OF GPR139 AND INVESTIGATING ITS POSSIBLE ROLE IN BRAIN DEVELOPMENT

G protein coupled receptors are a large family of cell surface receptors and are involved in a plethora of physiological functions from vision to various neuronal functions. They have been a major target in the pharmaceutical industry and more than one third of currently available drugs target a GPCR. Although extensively studied, there are still 140 orphan GPCRs. GPR139 is an orphan GPCR in the rhodopsin family and is primarily expressed in medial habenula. In addition to its cognate ligand, its function is still not known. At the time of the initiation of our study, the literature only suggested a possible role of GPR139 in neurological disorders such as ADHD and Alzheimer's disease. Objective of this study is to investigate possible the role(s) of GPR139 in brain development via employing a *Gpr139* knock-out mice model, and via *in vivo* ablation of *Gpr139* in adult mice, and subjecting the animals to a set of behavioral experiments to measure the impact of deletion and ablation, respectively. In addition to animal experiments, various bioinformatic analyses were also performed to further characterize *Gpr139*. Our findings showed that *Gpr139* is expressed differentially in the brain tissue during embryonic development and its expression is most likely controlled by histone modifications and not DNA methylation. We also showed that ablation of GPR139 does not have any significant effects on spatial learning, locomotor activity, recognition memory and anxiety.

ÖZET

GPR139'UN KARAKTERİZASYONU VE BEYİN GELİŞİMİNDEKİ OLASI GÖREVLERİNİN ARAŞTIRILMASI

G protein ilintili reseptörler oldukça geniş bir hücre yüzeyi reseptör ailesidir ve görüşten çeşitli nörolojik fonksiyonlara kadar çeşitli görevler üstlenirler. GPCRlar ilaç sanayi için önemli bir hedeftir ve şu anda piyasadaki ilaçların üçte birinden fazlası GPCRları hedefler. Oldukça yoğun bir şekilde araştırılmalarına rağmen, hala 140 kadar yetim GPCR bulunmaktadır. GPR139, rodopsin ailesine ait bir yetim GPCR'dır ve medyal habenulada anlatıma sahiptir. Doğal ligandı hala bilinmemekle birlikte, üstlendiği görev de henüz bilinmemektedir. Çalışmalarımızın başladığı zamanlarda GPR139'un olası görevleri için literatür kaynakları dikkat eksikliği ve hiperaktivite bozukluğu, Alzheimer Hastalığı gibi nörolojik hastalıkları belirtmekteydi. Çalışmamızın amacı, GPR139'un beyin gelişimindeki olası etkilerini bir *Gpr139* knock-out fare modeli oluşturarak ölçmek, ve yetişkin beyinlerindeki görevini ise *in vivo* ablasyon ile tespit etmektir. Deneyler sonunda hayvanlar çeşitli davranış deneylerine tabi tutularak gen silme ve ablasyonun etkileri ölçüldü. Bu deneylere ek olarak *Gpr139*'un daha iyi karakterize edilebilmesi için çeşitli biyoenformatik analizler de gerçekleştirildi. Elde ettiğimiz sonuçlara göre *Gpr139* geni, embriyonik gelişme sürecinde beyin dokularında günlere göre farklı anlatıma sahiptir. Bu farklı anlatım DNA metilasyonu ile değil, büyük ihtimalle histon modifikasyonları ile kontrol edilmektedir. Ayrıca, GPR139 ablasyonunun farelerde uzamsal öğrenim, lokomotor aktivite, tanıma hafızası ve endişe üzerinde anlamlı bir etkisi yoktur.

TABLE OF CONTENTS

LIST OF FIGURES

LIST OF TABLES

LIST OF SYMBOLS

A	Adenine
C	Cytosine
^{o}C	Centigrade Degree
G	Guanine
g	Gravity
m	Meter
M	Molar
ml	Mililiter
mM	Milimolar
ng	Nanogram
nl	Nanoliter
T	Thymine
V	Volt
w	Weight
Y	Tyrosine
u	Unit
α	Alpha
β	Beta
γ	Gamma
δ	Delta
µg	Microgram
µl	Microliter
µM	Micromolar

LIST OF ACRONYMS/ABBREVIATIONS

APC	Adenomatous polyposis coli gene product
APS	Ammonium peroxidisulfate
BRG	Brahma-related gene
$CaCl_2$	Calcium chloride
cAMP	Cyclic adenosine mono phosphate
cDNA	Complementary deoxyribonucleic acid
CHIP	Chromatin immunoprecipitation
CO_2	Carbondioxide
CRD	Cysteine rich domain
CsCl	Cesium chloride
DEPC	Diethylpyrocarbonate
DMEM	Dulbecco's modified Eagle's medium
DMSO	Dimethyl sulfoxide
DNA	Deoxyribonucleic acid
DNase	Deoxiribonuclease
DPH	DEPC treated water
DTT	Dithiothreitol
EDTA	Ethylenediaminetetraacetic acid
EMBO	European Molecular Biology Organization
EMSA	Electro mobility shift assay
ERLB	EtBr RNA loading buffer
EtBr	Ethidium bromide
EtOH	Ethanol
FBS	Fetal bovine serum
FCS	Fetal calf serum
GFP	Green flourescent protein
GITC	Guanidium isothiocyanate
GPCR	G-protein coupled receptor
GPR139	G-protein coupled receptor 139

GPR142	G-protein coupled receptor 142
GTP	Guanosine triphosphate
KCl	Potassium chloride
LB	Luria-Bertani
LiCl	Lithium chloride
$MgCl_2$	Magnesium chloride
$MgSO_4$	Magnesium sulphate
MOPS	Morpholino propane sulfonic acid
mRNA	Messenger ribonucleic acid
NaCl	Sodium chloride
NaOAc	Sodium Acetate
NaOH	Sodium hydroxide
NCBI	National Center for Biotechnology Information
NLS	Nuclear localization sequence
oGPCR	Orphan G-protein coupled receptor
OD	Optical density
PAGE	Polyacrylamide gel electrophoresis
PBS	Phosphate buffered saline
PCR	Polymerase chain reaction
PKC	Protein kinase C
QRT-PCR	Quantitative reverse transcriptase mediated PCR
RGS	Regulator of G-protein signaling
RNA	Ribonucleic acid
Rnase	Ribonuclease
RPM	Revolutions per minute
RT-PCR	Reverse transcriptase-polymerase chain reaction
SDS	Sodium dodecyl sulphate
SOB	Super optimal broth
SOC	Super optimal catabolite repressed broth
TAE	Tris-acetic acid EDTA
TAK	TGF-beta activated kinase

TBE	Tris base EDTA
TEMED	N,N,N,N-tetramethylethylenediamine
TES	Tris-EDTA sodium chloride
TPM	Transcript per million

1. INTRODUCTION

1.1. G Protein Coupled Receptors

1.1.1. Structure and Function

The G protein coupled receptors (GPCRs) superfamily constitute the largest family of cell surface receptors with about than 800 genes, which represents about 2-3% of all protein coding genes in the human genome (Figure 1.1) [1]. They are defined by their ability to interact with a G protein and presence of seven transmembrane domain sequences [1]. GPCRs act through heterotrimeric G proteins to transduce paracrine, endocrine or exocrine stimuli including peptides, nucleosides, nucleotides, odorants, small chemicals, lipids and photons [2, 3].

Despite the diversity in the structure of their ligands, GPCRs share a common molecular feature: they are composed of seven transmembrane α helices connected by three intracellular and three extracellular loops. Their C termini is intracellular and N termini is extracellular [4].

GPCRs are expressed in wide variety of human tissues and play various physiological roles [5]. Over 50% of GPCRs are involved in sensory functions including vision, olfaction and sense of taste [6]. Majority of the remaining non-sensory GPCRs are expressed in the brain and play roles in neurological processes including cognition [7].

GPCRs have been a major interest in pharmacological studies due to their physiological roles in development and adulthood, and are targets for more than 34% of currently marketed drugs [8].

Endogenous ligands of more than 140 GPCRs, dubbed orphan GPCRs (oGPCR), are still not known [9]. These oGPCRs are of great interest by the scientific and pharmaceutical industry, and being actively researched.

They pose great opportunities in understanding human physiology and discovery of potential therapeutic mechanisms [10]. With new findings, the number of GPCRs actively targeted by drugs for treatment of various diseases is expected to increase.

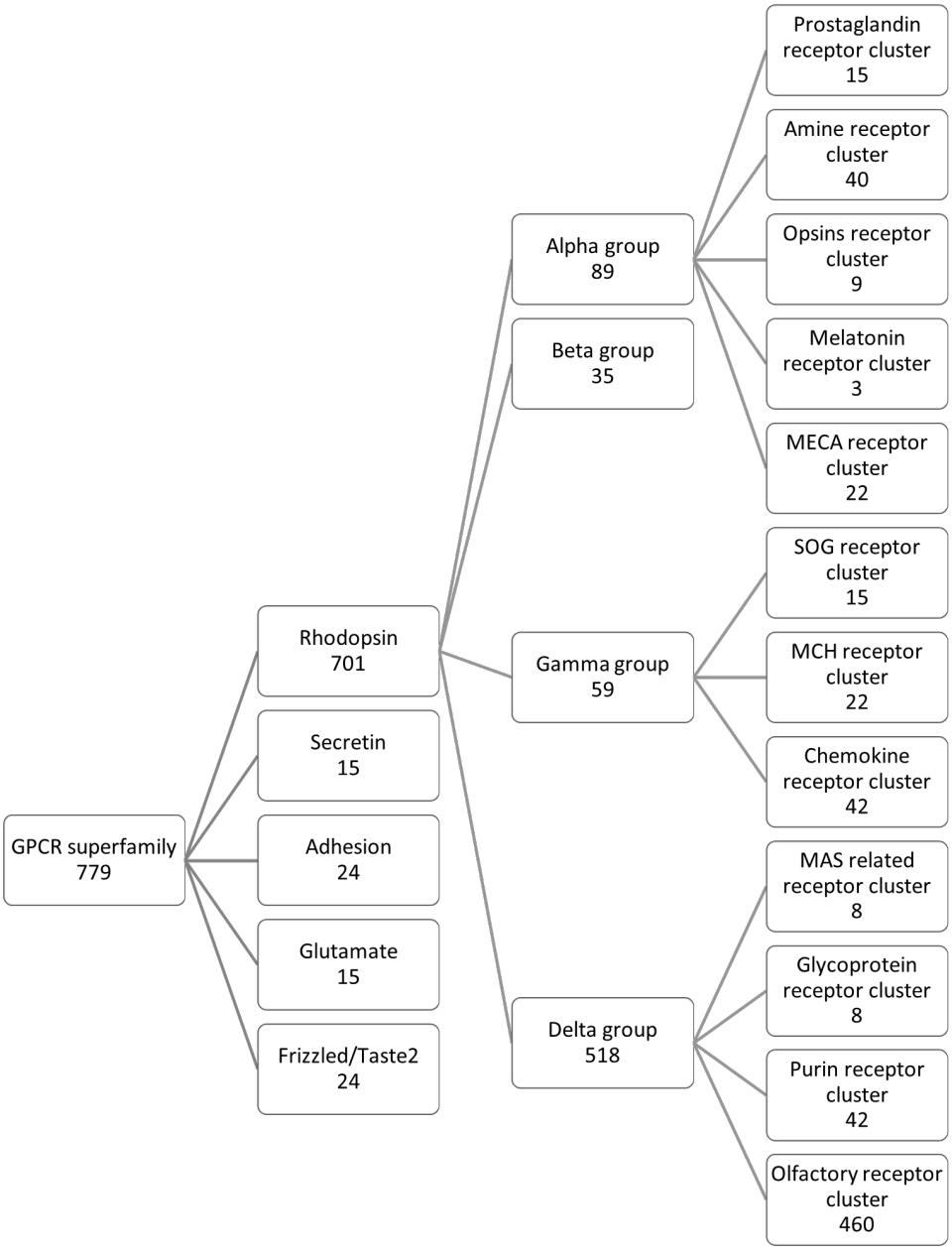

Figure 1.1. Classification of GPCRs and number of receptors in each category. Figure is created using data in Fredriksson et al. (2003) [1].

1.1.2. GPCR Signaling

1.1.2.1. G Protein Dependent Signaling. GPCRs can act through G$\alpha\beta\gamma$ protein coupling. Upon activation, the GPCR promotes the exchange of guanosine diphosphate (GDP) bound to the alpha subunit with guanosine triphosphate (GTP) molecule. This exchange results in dissociation of the G$\beta\gamma$ dimer and Gα monomer. Dissociated G$\beta\gamma$ and Gα subunits can then bind to various effectors to promote signalling (Figure 1.2).

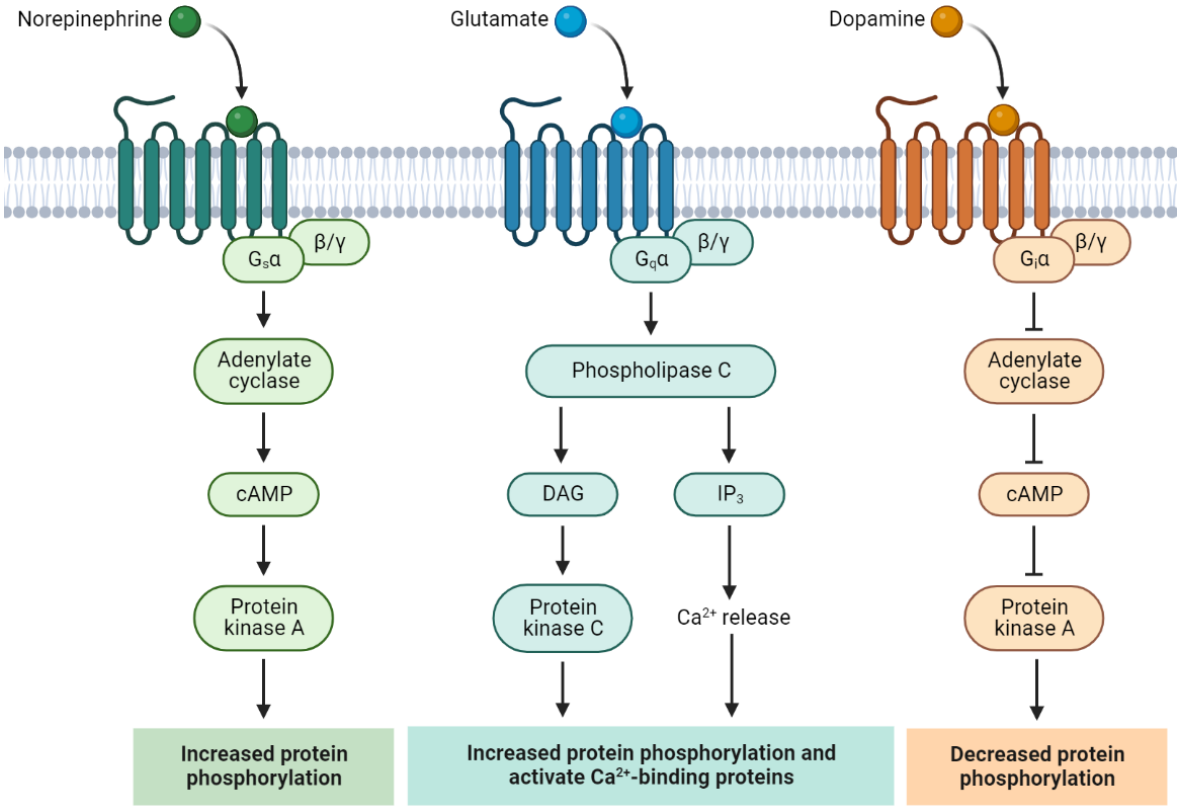

Figure 1.2. G protein dependent signaling of GPCRs for Gα_i, Gα_s, and Gα_q.

Gα proteins mainly determine the signaling properties. There are four subclasses of Gα proteins based on their sequence homologies and functional similarities.

$G\alpha_{q/11}$ class consists of $G\alpha_q$, $G\alpha_{11}$, $G\alpha_{14}$ and $G\alpha_{15}$ proteins. When activated they result in activation of phospholipase C β (PLC-β) enzymes, which in turn hyrdolyse phosphatidylinositol 4,5-bisphosphate (PIP_2) into inositol 1,4,5-trisphosphate (IP_3) and diacylglycerol (DAG). IP_3 promotes the flux of Ca^{2+} from the endoplasmic reticulum (ER) to the cytoplasm while DAG activates the protein kinase C (PKC).

$G\alpha_s$ is comprised of $G\alpha_s$ and $G\alpha_{olf}$. $G\alpha_{olf}$ is mainly expressed in the olfactory system. Upon activation, $G\alpha_s$ stimulates adenylyl cyclase which then converts adenosine triphosphate (ATP) to 3′,5′-cyclic adenosine monophosphate (cAMP). cAMP acts as a secondary messenger to activate protein kinase A (PKA). PKA can then stimulate various downstream effectors to induce various pathways.

$G\alpha_{i/0}$ family acts in opposition of the $G\alpha_s$ proteins, namely inhibiting the cAMP dependent pathway via inhibiting adenylyl cyclase activity.

$G\alpha_{12/13}$ proteins are the least characterized G proteins due to lack of secondary messengers which allows measuring the G protein activity. They activate Rho-guanine nucleotide exchange factors (RhoGEFs) which mediates GDP-GTP exchange in Rho small GTPases.

$G\beta\gamma$ dimers can also stimulate downstream effectors such as mitogen activated protein kinase (MAPK) and certain types of adenylyl cyclases.

1.1.2.2. G Protein Independent Signaling. β-arrestins were classically categorized as the inhibitor of GPCR signaling via steric hindrance and internalization of the receptors. In recent years, however, it has been shown that β-arrestins can promote downstream signaling such as activation of ERK2 mitogen-activated protein kinase. Moreover, some GPCRs have shown to continue signaling even after β-arrestin mediated internalization (Figure 1.3).

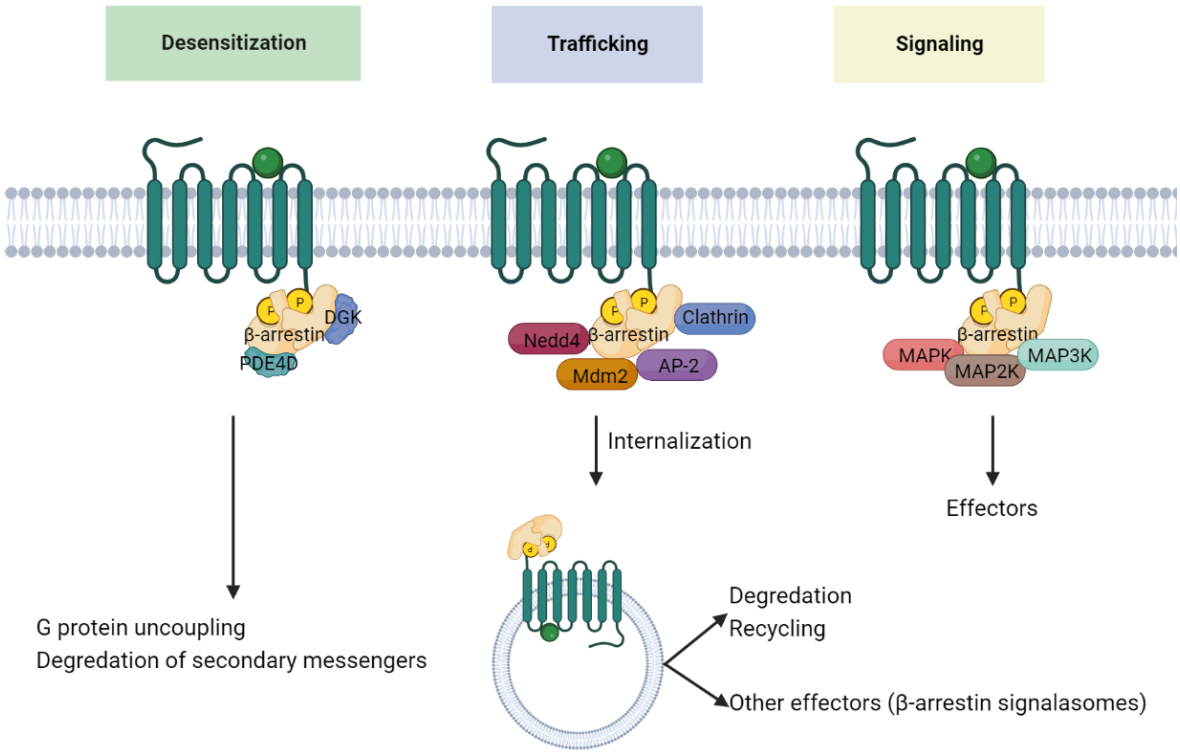

Figure 1.3. G protein independent signaling of GPCRs. GPCRs can continue signaling via different effectors when internalized via β-arrestin mediated internalization, or still localized to the cellular membrane to stimulate various pathways.

1.1.3. Role of G Protein Coupled Receptors in Brain Development and Cognition

Brain development is a complex and long process involving several distinct stages through pre and post-natal life of the organisms [11]. More than 90% of the 370 non-sensory GPCRs are expressed in the brain tissue [6] and they have been associated with various processes of brain development including cortical development [12], synapse development [13], dendritic maturation and stability [14], neural tube closure, neurite growth, neuronal migration [15], and axonal guidance [16].

In addition to neurodegenerative disorders, GPCRs are involved in the pathophysiology of various neurodegenerative disorders including Alzhaimer's Disease, dementia, Parkinson's Disease and Huntington's Disease [7].

Among the oGPCRs, 78 of them are shown to be expressed in the mouse brain and have functions in cognition, mood and motivation [17]. Considering involvement of GPCRs in brain development, function and pathophysiology of neurodegenerative disorders, studies aiming to discover the function and ligands of oGPCRs, and find new treatment courses for developmental and cognitive disorders are surely valuable.

1.2. GPR139 Receptor

GPR139 is an orphan GPCR of the Rhodopsin family. It was first reported by bioinformatics analysis of human genome as a local duplicate of its discovery twin GPR142 [1] and later reported as a separate GPCR by three groups [3, 5, 18]. It shows 50% sequence identity with GPR142 and at most 20-25% identity with other rhodopsin family GPCRs [18]. It is primarily expressed in distinct areas of the central nervous system (CNS) especially in habenula, medulla, putamen and caudate nucleus [18, 19]. It is also expressed in mouse embryo showing different mRNA levels between E11, E15 and E17 [18].

GPR139 remains to be an orphan receptor, meaning its endogenous ligand(s) and the pathway(s) in which it takes part remain to be discovered. Brain extracts have been shown to contain its cognate ligand and it is speculated to be a small peptide [18] but have not been identified. Its expression pattern in CNS in adults is consistent with a possible role in regulation of locomotor activity [19]. This is supported by a study in which Gpr139 agonist shown to reduce locomotor activity in rats [20]. Other studies showed a correlation between attention deficit hyperactivity disorder (ADHD) [21], inattention [22] and variations in GPR139 locus. It is also thought to be a possible contributor in etiology of Parkinson's disease (PD) [19, 23].

Therefore, at the time of the beginning of this study, GPR139 was of interest for pharmacological research and several small molecule agonists and antagonists for GPR139 have already been identified and synthesized [10, 20, 24–26].

1.2.1. GPR139 Expression

GPR139 mRNA expression is localized to the central nervous system in mice, rats, and humans [5, 20, 27]. Studies targeting the protein expression in mice shown localization to habenula [20]. Expression level of the receptor in the brain is found to be low via radiolabelled agonist study [28].

Habenula is an evolutionarily conserved structure and is present in the diencephalon of all vertebrates [29]. It is involved in nociception, learning, reproduction, sleep-wake cycle, stress response and nutrition [30] and involved in control of both dopaminergic and serotonergic systems [29]. Although lateral habenula is currently seeing a new wave of interest after the initial interest in 70s and 80s following reports outlining its involvement in negative reward response, medial habenula is still not in the focus of the scientific community [31]. Medial habenula is the only known structure in the brain with functional NMDA receptor GluN1/GluN3A [32] which is involved in learning and memory [33].

1.2.2. Putative Endogenous Ligands of GPR139

Brain extracts have been shown to contain the endogenous ligand of GPR139 [18]. Its cognate ligand is thought to be a small peptide [18]. Further studies have shown L-Phe to be an agonist of GPR139 [10] with EC50 value of 330 µmole/L. The L-Phe concentration is in the range of 60 to 200 µmole/L in wild type mice [34]. According to Isberg et. al. (2014), 80 µmole/L L-Phe concentration results in $\leq$10% activation. Even though EC50 value of L-Phe could be different in-vivo, these findings suggest that L-Phe is not likely an endogenous ligand of GPR139.

In theory, L-Phe can be stored and released in high concentrations as a neurotransmitter to activate GPR139 but this is yet to be determined. L-Trp (EC50 = 220 μmole/L) was also suggested as a possible ligand of GPR139. Derivatives of these amino acids, β-phenylethylamine, tryptamine and amphetamine were also shown to activate GPR139 at μM ranges [12]. Endogenous ligand of GPR139 is yet to be determined.

1.2.3. Action Mechanism

The mechanism through which GPR139 acts is largely unknown. There are numerous proposed mechanisms of action which involve dimerization [18] or acting as a monomer [5,18,20,25] and interact with $G_{q/11}$ [5,10,23,26], $G_{12/13}$ [5], G_i [18] or G_s [25]. The consensus is leaning towards $G_{q/11}$ mediated activity.

1.2.4. Putative Roles of GPR139

The physiological role of GPR139 is still not known. Related publications suggest four possible functions based on its expression profile and functional studies performed on animal models.

Structure analysis and agonist studies suggest that aromatic peptides can stimulate GPR139, which leads to the hypothesis that GPR139 acts as a peptide receptor in the brain. This hypothesis, however, needs further functional evidence. The stimulation of GPR139 by high concentrations of L-Phe leads scientists to investigate the potential role of over-stimulation of GPR139 in aetiology of phenylketonuria [24].

GPR139 has expression in the striatum in humans, mice and rats [5,18,20]. Since striatum is necessary for voluntary movement, it is speculated that GPR139 may be involved in locomotor activity.

There are publications in the literature supporting this speculation. None of them, however, can clearly show or claim a direct relation between the GPR139 and locomotor activity. Liu et. al. (2015) has treated male Sprague Dawley rats with a small molecule agonist for GPR139 (JNJ-63533054, EC50: 16 nM) and observed reduced locomotor activity. The authors refrained from claiming a direct correlation from the administration of agonist and reduced locomotor activity due to possible sedative effects of the procedure.

As mentioned above, L-Phe has been discovered as an agonist of GPR139 [10]. EC50 value for L-Phe is found to be 330 μmole/L. This value is much higher than physiological concentrations of L-Phe in the brain (50-80 μmole/L) [35]. Authors reported that the calculated EC50 value falls in the range they found to activate the receptor and suggested GPR139 may play a role in monitoring fluctuations on this amino acid [10]. Upon closer inspection of their data, it is seen that 80 μmole/L L-Phe results in $\leq$10% activation. Even though EC50 value of L-Phe could be different in-vivo, these findings suggest that L-Phe is not likely an endogenous ligand of GPR139. In another study, dopaminergic midbrain neurons are shown to be protected against Rotenone toxicity by GPR139 agonist treatment [19]. In an earlier patent application for a GPR139 knockout mouse strain, GPR139 knockout mice was reported to have significantly lower scores in rotarod performance test, which is used to measure motor coordination and balance [36]. These publications suggest that GPR139 might have a role in regulation of locomotor activity, which is highly disrupted in PD.

The interest in GPR139 was largely based on its possible role in PD due to its potential value as a pharmaceutical drug target. It is, however, also shown that Gpr139 is widely expressed in E18.5 mouse brain at mRNA level [18], namely CA1 area of hippocampus, median habenular nucleus, lateral habenular nucleus, nucleus oculomotoris, nucleus hypoglossis, piriform, entorhinal cortices, lateral septum, amygdala, median thalamic nuclei, reticular nucleus of thalamus, central gray, inferior colliculus, medial vestibular nucleus and inferior olive. This wider expression pattern compared to adult brain suggests that Gpr139 may play a role in brain development. This is further supported by its expression at different levels at different embryonic stages.

Latest publications on GPR139 are focusing on its effect on μ-opioid receptor (MOR). GPR139 has been shown to oppose the activity of MOR by forming a heterodimer with MOR or via its signaling through $G_{q/11}$ [37, 38]. Heterodimerization of GPR139 and MOR is shown to reduce the amount of MOR on the cell surface by inducing β-arrestin mediated internalization of MOR [37]. Another publication shown the $G_{q/11}$ signaling of GPR139 alone can be sufficient to reduce MOR mediated signaling in habenula [38]. These current findings opened way for novel treatments of opioid addiction and withdrawal effects by using GPR139 agonists. In addition to its possible role in opioid addiction regulation, there is an ongoing phase I clinical trial investigating a GPR139 agonist as a possible treatment for schizophrenia [39].

While GPR139's potential role in PD, schizophrenia and/or modulation of MOR activity is not devalued by its possible role in brain development, but this possibility opens a new venue for investigation that remains largely unexploited.

2. PURPOSE

G-protein coupled receptors are major targets for drugs for various diseases with more than 34% of all FDA approved drugs targeting a GPCR. Orphan GPCRs are currently being investigated thoroughly both in terms of their function and their agonist and antagonists as potential drugs.

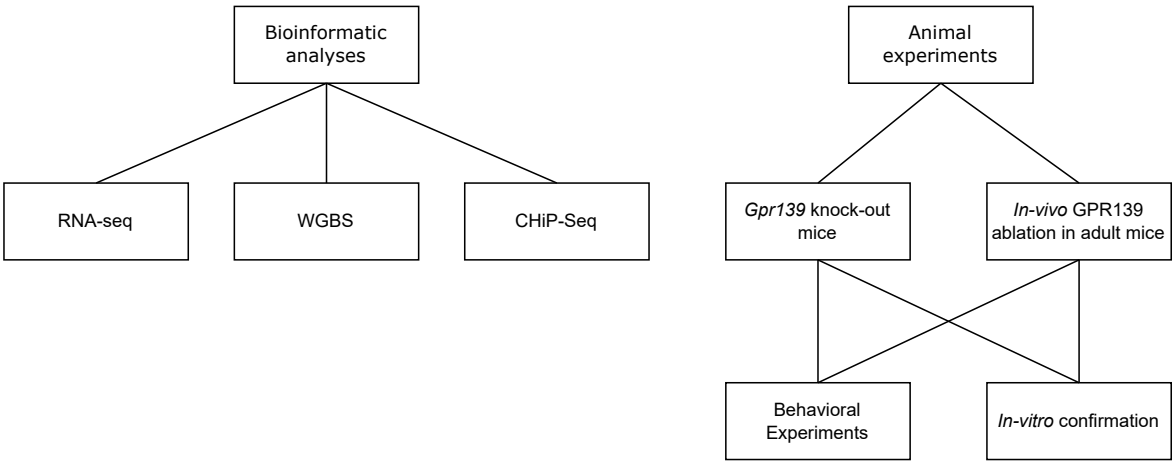

Figure 2.1. Simplified workflow of the study.

In this study, the primary goal was to investigate the possible role of GPR139 in brain development by creating a *Gpr139* knock-out mouse strain and examine various variables such as morphological changes of the brain, changes in transcriptome and proteome compared to wild type mice. For the same purpose, in addition to the creation of the knock-out mouse strain, *in vivo* ablation *Gpr139* in adult mice using intracranial injection of adenoassociated virus containing Cre recombinase and sgRNA targeting *Gpr139* into FloxP-Cas9 adult mice. Knock-out and *Gpr139* ablated mice were then going to be used subjected to behavioral tests to assess possible effects of *Gpr139* on behavior. Various experiments were conducted for further characterization of the receptor including bioinformatic analyses by data-mining public databases and projects such as ENCODE [40] were conducted to examine the expression pattern, differential methylation levels of CpG's and histones.

3. MATERIALS

3.1. Chemicals

All laboratory chemicals were analytical grade from Sigma (St. Louis, MO, USA), Merck (Schucdarf, Germany) or Apllichem (Darmstadt, Germany) unless stated otherwise in the text. Tissue culture media and solutions were purchased from Invitrogen (San Diego, CA USA) and Biochrom AG (Berlin, Germany). In vitro transfection reagent, Turbofect was purchased from Fermentas (Burlington, Canada).

3.2. Buffers and Solutions

3.2.1. Electrophoresis and Western Blotting Buffers and Solutions

50X Tris-acetic acid EDTA (TAE)	242 g Tris Base 100 mL of 0.5 M pH 8.0 EDTA 57.1 ml glacial acetic acid Distilled water up to 1 L pH 7.8
Ethidium bromide (EtBr)	1 mg/ml (stock solution) 0.5 μg/ml (working solution)
DNA Loading buffer & 6X loading buffer	Purchased from Fermentas (Burlington, Canada)

12.5 per cent SDS-PAGE gel (running gel)	12.5 per cent acrylamide : bisacrylamide (39:1) 375 mM Tris-HCl (pH 8.8) 0.1 per cent SDS 0.1 per cent Ammonium persulfate (APS) 0.1 per cent TEMED
3.5 per cent SDS-PAGE gel (stacking gel)	3.5 per cent acrylamide : bisacrylamide (39:1) 125 mM Tris-HCl (pH 6.8) 0.1 per cent SDS 0.1 per cent APS 0.1 per cent TEMED
6X SDS-PAGE sample buffer	80 mM Tris-HCl (pH 6.8) 30 per cent glycerol 10 per cent SDS 0.6 M DTT 0.012 per cent bromophenol blue
5X SDS electrophoresis buffer	0.125 M Tris base 0.96 M glycine 0.5 per cent SDS
Western blot lysis buffer	150 mM NaCl 5 mM EDTA 1 per cent Triton X 100 10 mM Tris-HCl pH 7.4 5 mM DTT 0.1 mM PMSF

Transfer buffer	25 mM Tris 200 mM Glycine 10 per cent methanol
Colloidal coomassie stock solution	2 per cent (w:v) coomassie brilliant blue G250 0.2 g/l sodium azide
Colloidal coomassie fixing solution	50 per cent ethanol 2 per cent phosphoric acid
Colloidal coomassie equilibration solution	2 per cent phosphoric acid 18 per cent ethanol 15 per cent (w:v) ammonium sulfate
Colloidal coomassie destaining solution	1 per cent acetic acid
Ponceau S staining solution	0.5 per cent Ponceau S (w:v) 1 per cent acetic acid
Tris buffered saline with Tween 20 (TBST)	150 mM NaCl 20 mM Tris-HCL (pH 8.0) 0.1 per cent Tween 20 0.01 per cent (w:v) sodium azide
Blocking solution	5 per cent non-fat milk in TBST

Equilibration buffer I	125 mM tris base, pH 6.8 1 per cent SDS 8.7 per cent glycerol 5 mM DTT
Equilibration buffer II	125 mM tris base, pH 6.8 1 per cent SDS 8.7 per cent glycerol 2 per cent iodoacetamide 0.005 per cent bromophenol blue

3.2.2. Bacterial Culture Buffers and Solutions

Luria-Beertani medium (LB)	10 g tryptophan 5 g yeast extract 10 g NaCl Distilled water up to 1 L, autoclaved
Luria-Bertani agar	10 g tryptophan 5 g yeast extract 10 g NaCl 15 g agar Distilled water up to 1 L, autoclaved
Ampicillin stock	100 mg/ml in 50 per cent ethanol Sterilized by filtration and stored at -20^{o}C 100 μg/ml working concentration

Chloramphenicol stock	30 mg/ml in absolute ethanol
	Sterilized by filtration
	Stored at -20^{o}C
	30 μg/ml working concentration
SOC	20 g tryptone
	5g yeast extract
	2 ml of 5M NaCl
	2.5 ml of 1M KCl
	10 ml of 1M $MgCl_2$
	10 ml of $MgSO_4$
	20 ml of 1 M glucose
	Distilled water up to 1 L
	Sterilized by filtration
	Stored at -20^{o}C

3.2.3. Immunofluorescence Buffers and Solutions

10X PBS	81.8 g NaCl 2 g KCl 14.2 g Na_2HPO_4 2.45 g KH_2PO_4 Up to 1 L with distilled water
1X PBST	1X PBS 0.5 per cent Triton X-100
20 per cent paraformaldehyde stock	10 g paraformaldehyde 50 µl of 10 M NaOH up to 50 ml with distilled water Heat to 65^{o}C to dissolve Store at -20^{o}C
4 per cent paraformaldehyde in PBS	10 ml 20 per cent paraformaldehyde 5 ml 10X PBS 35 ml distilled water
Blocking solution	3 per cent BSA in PBS
Cell permeabilization solution	1X PBS 0.5 per cent Triton X-100

3.3. Enzymes

Restriction enzymes, Taq DNA Polymerase and Pfu DNA Polymerase were purchased from Fermentas (Burlington, Canada) together with their respective reaction buffers. T4 DNA ligase was purchased from Promega (Madison, WI, USA). Trypsin (0.025 per cent, ready to use) was purchased from Invitrogen (San Diego, CA, USA).

3.4. Antibodies

Rabbit anti-GPR139 polyclonal antibody was purchased from Thermo Scientific (catalog no: PA5-33632), rabbit pan-actin polyclonal antibody was from Cell Signaling (catalog no: 4968), goat HRP anti-GFP antibody was from Abcam (ab6663), rabbit anti-Vinculin antibody was from Abcam (ab91459), sheep anti-mouse/HRP polyclonal antibody and donkey anti-rabbit/HRP polyclonal antibodies were purchased from Amersham (catalog no's: NA931 and NA934, respectively). Goat anti-mouse/Alexa Fluor®488 polyclonal antibody was from Invitrogen (catalog no: A-11001).

3.5. Western Blotting Reagents

Hybond-P nitrocellulose membrane and RCL Plus Western Blotting Detection Reagents were purchased from Amersham Biosciences (Upsalla, Sweden). Kaleidoscope pre-stained molecular weight marker was purchased from Biorad (Hercules, CA, USA).

3.6. Nucleic Acids

DNA molecular weight markers and deoxyribonucleotides were purchased from Fermentas (Burlington, Canada). Cas9 plasmid pSpCas9(BB)-2A-GFP (PX458) was a gift from Feng Zhang (Addgene plasmid 48138; RRID:Addgene_48138). Primers and oligonucleotides were purchased from Macrogen Inc. (Seul, Korea).

3.7. Bacterial strains and Mammalian Cell Lines

E. Coli bacterial strain DH5α was used for cloning purposes.

Human embryonic kidney cell line HEK293T was purchased from ABMGood (British Columbia, Canada) and used for AAV production.

3.8. Kits

QIAprep Spin Miniprep kit, Endofree Plasmid Maxi Kit, QIAquick Gel Extraction kit and RNeasy Mini Kit were purchased from Qiagen (Hilden, Germany). Dual-glo Luciferase assay kit and ImPromII Reverse Transcription System was purchased from Promega (Madison, WI, USA). LightCycler FastStart DNA Master SYBR Green I kit was from Roche (Basel, Switzerland). MEGAshortscript T7 and mMESSAGE mMACHINE T7 ultra kits were purchased from Thermo Fischer Scientific (Massachusetts, United States) used for *in vitro* transcription of sgRNA scaffolds and Cas9 mRNA, respectively.

3.9. Equipment

Autoclave	Midas 55, Prior Clave, UK
Balances	DTBH 210, Sartorius, GERMANY
	Electronic Balance VA 124, Gec Avery, UK
Carbon dioxide tank	2091, Habas, TURKEY
Cell culture incubator	Hepa Class 100, Thermo, USA
Centrifuges	Ultracentrifuge J2MC, Beckman Coulter, USA
	Mini Centrifuge 17307-05, Cole Parmer, USA
	Centrifuge 5415R, Eppendorf, USA
	Centrifuge, Allegra X-22, Beckman Coulter, USA
Deepfreezers	-20^{o}C, Arçelik, TURKEY
	-70^{o}C Freezer, Harris, UK
	-86^{o}C ULT Freezer, ThermoForma, USA
Documentation Systems	Gel Doc XR System, Bio-Doc, ITALY
	Stella Imaging Station, Raytest, GERMANY
Drummond Wiretrol II Calibrated Micropipette	Drummond, USA
Electrophoresis Systems	Mini-sub Cell GT, Biorad, USA
	Mini-Protean III Cell, Bio-Rad, ITALY
	Ettan IPGphor 3, GE Healthcare, UNITED KINGDOM
Hand tally counter	Milky Way Counter, TAIWAN
Heat blocks	DRI-Block DB-2A, Techne, UK
Hemocytometer	Improved Neubauer, Weber Scientific International Ltd, UK
Laminal flow cabinet	Labcaire BH18, UK
Magnetic Stirrers	M221 Elektro-mag, TURKEY
	Clifton Hotplate Magnetic Stirrer, HS31, UK
Micro-drill	Istanbul Diş Deposu, TURKEY

Micropipettes	Finnpipette, Thermo, USA
Microplate Reader	680, Biorad, USA
Microscope	Inverted Microscope, CKX41, Olympus, JAPAN
	Invervet Microscope, Observer.Z1, Zeiss, GERMANY
Microwave oven	M1733N, Samsung, MALAYSIA
One-axis Oil Hydraulic Micromanipulator	Narishige, JAPAN
OptiSeal Tubes	Thermo Scientific, USA
pH meter	WTW, GERMANY
Pipettor	Pipetus-akku, Hirscmann Labogerate, GERMANY
Power Supply	Biorad, USA
Real Time PCR	LightCycler 1.5,
	Diagnostics, SWITZERLAND
Refrigerators	2082C, Arçelik, TURKEY
	4030T, Arçelik, TURKEY
Shakers	VIB Orbital Shaker, InterMed, DENMARK
	Lab-Line Universal Oscillating Shaker, USA
Software	Quantity One, Bio-Rad, ITALY
	Light Cycler 4.0 Analysis Software,
	Roche Diagnostics, SWITZERLAND
	ImageJ, Image Analysis Software,
	(http://rsb.info.nih.gov/ij/)
	Progenesis SameSpots, Nonlinear Dynamics, UK
	AxioVision, Zeiss, GERMANY
Spectrophotometer	Agilent 8453, USA
	NanoDrop 1000, USA
Syringe	701N 26S/51/2, Hamilton, SWITZERLAND

Thermocyclers	Gene Amp. PCR System 2700, Applied Biosystems, USA
Vacuum pump	KNF Neuberger, USA
Vibratome	Leica, GERMANY
Vortex	Vortexmixer VM20, Chiltern Scientific, UK
Water baths	TE-10A, Techne, UK
Water purification	WA-TECH ultra pure water purification system, GERMANY

4. METHODS

4.1. General Molecular Techniques

4.1.1. Preparation of Chemically Competent E. coli and Transformation

Five ml of LB medium with 25 μg/ml streptomycin was inoculated with 100 μl *E. Coli* strain DH5α glycerol stock and grown overnight at 37^{o}C with shaking at 200 rpm. The next day, 25 ml LB medium was inoculated with 250 μl of the overnight culture and grown untill OD 595 reached between 0.4 and 0.6. Cells were centrifuged for 10 minutes at 3000 g at 4^{o}C. Obtained pellet was resuspended in 12.5 ml of ice-cold sterile 50 mM $CaCl_2$ and incubated on ice for 30 minutes. Cells were centrifuged again using the same conditions and pellet was resuspended in 2.5 ml ice-cold sterile 50 mM $CaCl_2$. 50 μl of this preparation was used for transformations. For long term storage, glycerol was added to 10 per cent final concentration and the cells were snap-frozen in liquid nitrogen and stored at -80^{o}C.

For transformation 100 μl of the competent cells were thawed on ice for 15 min and 1 μl of plasmid was added and gently stirred with the help of the micropipette tip. Cells were then incubated on ice for 20 minutes, then placed in 42^{o}C heat-block for 1 minutes and then immediately on ice for 2 minutes. 500 μl of room temperature SOC medium was added and cells were incubated for 1 hour at 37^{o}C with shaking at 200 rpm. 100 μl of the cell suspension was spread on selective plates containing appropriate antibiotic and grown overnight at 37^{o}C. Colonies with plasmids and/or desined insertions were detected using colony PCR. For colony PCR, a sample of the colony was sampled using a sterile pipette tip and the tip is dipped into the PCR reaction mix (Table 4.1).

PCR reaction was carried out using the cycle program in Table 4.2.

Table 4.1. Colony PCR reaction mixture.

Reagent	Amount
PCR buffer (10X)	2.5 µl
dTNP mix (25 mM each)	0.2 µl
Forward primer	0.5 µl
Reverse primer	0.5 µl
Taq polymerase	21.2 µl
ddH_2O	7 µl

Table 4.2. Colony PCR thermal cycler program.

Temperature	Duration	Cycles
95^{o}C	5 min	1
95^{o}C 52^{o}C 68^{o}C	30 sec 20 sec 20 sec	20
68^{o}C	5 min	1
24^{o}C	hold	

4.1.2. Plasmid Purification

All plasmid purifications were done using Qiagen's QIAprep Spin Miniprep Kit, Plasmid Midi Kit or Thermo Scientific's GeneJET Plasmid Miniprep Kit following manufacturer's protocol. Concentrations and qualities of plasmids were checked by spectrophotometric measurements and by agarose gel electrophoresis. OD 260/280 ratio was between 1.8 and 2.0. Only endofree preparations of plasmids were used for transfections.

4.1.3. Polymerase Chain Reactions

Unless stated otherwise, touchdown PCR technique was used for polymerase chain reactions used in this study. Primer pairs are designed using Primer3-Plus software [41] and Tm values were calculated using online NEB TM Calculator Tool (https://tmcalculator.neb.com/) using appropriate polymerase enzyme and buffer compositions. Denaturation and extension temperatures and durations are used as manufacturer's recommendations. Annealing temperatures were started 5-10^{o}C above the recommended Tm values by NEB TM Calculator Tool and reduced by 1^{o}C per step until reaching 3-4^{o}C below the recommended Tm value. Final annealing temperature was kept until reaching the desired cycle count, typically between 25 and 35 depending on the input material and the purpose of the PCR.

4.1.4. Agarose Gel Electrophoresis

DNA fragments were resolved on standard 1X TAE agarose gels. The percentage was determined by the length of the DNA fragment to be run and was between 1 per cent and 2 per cent. Agarose powder was melted in 1X TAE buffer by heating in a microwave oven and after cooling the solution to room temperature ethidium bromide was added to a final concentration of 0.5 µg/ml. Samples were prepared by adding either 6X BPB-loading dye or 6X OrangeG-loading dye for amplicons above or below 250 bps, respectively. Gels were run in 1X TAE buffer at constant voltage until the dye front migrated to desired distance. Gels were visualized under UV light using the GelDoc image documentation system (BioRad, USA).

4.1.5. Gel Purificaiton of DNA Framgents

DNA bands of interest are excised from the agarose gel using a scalpel and transferred to 2 ml centrifuge tube. The tubes were weighed before and after to determine the weight of the gel slab. DNA fragments were then isolated using GeneJET Gel Extraction Kit (Thermo Scientific) following manufacturer's protocol. Resulting isolates were checked for quality and quantity using NanoDrop.

4.1.6. SDS-PAGE Electrophoresis and Western Blotting

Mini-Protean III cell and Mini-Transblot cell (Biorad) were used for SDS-PAGE gel preparation, running and transfer. For western blotting, 10 per cent separating gels were cast up to 3 cm from the top of the gel cassettes and layered with 0.1 per cent SDS in distilled water and left for polymerization. After 30 minutes SDS layer was poured off and rinsed with dH_2O and 3.5 per cent stacking gel was poured. Combs of appropriate width and size were inserted immediately after casting stacking gel and any trapped air bubbles were removed to obtain perfectly shaped wells. Samples were lysed with SDS lysis buffer, centrifuged for 5 minutes at 4^oC to pellet cell debris and mixed with appropriate volume of 6X SDS-PAGE loading dye. After heating at 95^oC for 10 minutes they were vortexed and flash-centrifuged and loaded into the wells. 5 µl of Kaleidoscope pre-stained marker (BioRad) was used as molecular weight estimate. Two gels were run in the same electrophoresis chamber applying 50 V until the BPB front entered the separating gel and the voltage increased to 100 V. Runs were stopped when BPB has left the gel or was about to reach the end of the gel.

For blotting the SDS-PAGE gels were removed from the cassette and stacker gels were discarded. Remaining separating gels, nitrocellulose membranes, sponges and blotting papers were immersed in transfer buffer for 10 minutes. The transfer cassettes were assembled and put in blotting chamber. Transfers were performed in cold room (4^oC) and with iceblock supplied with the Trans-blot cell and with stirring. Proteins were transferred onto PVDF membranes for 1 hr at 100 V. After the transfer the cassettes were disassembled, and the transfer efficiency was checked by the complete transfer of the prestained marker onto the membrane and then with Ponceau S staining and TBST was used for destaining. After the membranes were completely destained, 5 per cent non-fat milk in TBST was used to block the blots for 1 hr at room temperature or over night at 4^oC with shaking at about 100 rpm. Blots were then washed with TBST for 5 minutes and incubated with primary antibodies following manufacturer's dilution recommendations.

Primary antibodies were washed three times with TBST for 5 minutes each with shaking at 100 rpm and followed by secondary HRP conjugated antibodies following manufacturer's suggested procedures. Secondary antibodies were washed three times with TBST for 5 minutes. For detection, ECL Plus Western Blotting Detection Reagents (Amersham) were used to develop the blots and analyzed using Stella Imaging Station (Raytest). Images were quantified using ImageJ software.

4.2. Preparation of CRISPR/Cas9 Plasmids

Plasmids required for generation of *Gpr139* knock-out mice were prepared following the protocol by Yang, et al. (2014) [42] with the exception of designing of the targeting components.

4.2.1. Design of Targeting Components

Sequence of mouse *Gpr139* gene was obtained from Ensembl database [43]. Full sequences of exons 1 and 2 are extracted as well as 50 bp flanking regions from 3' and 5' sequences were submitted to the CRISPOR tool [44] using mouse genome version USCS Dec. 2011 and 20 bp - NGG protospacer adjacent motif (PAM) for Cas9.

Guide sequences generated by CRISPOR were then ranked by their specificity score and three sequences for each intron are selected based on:

- Their specificity score
- Position on the sequence (in intron, in intron-exon junction, in UTR)
- Out of frame score (prediction of percentage of clones that will carry out-of-frame deletions)
- Number of off-targets in the exome

Among 79 and suggested guide sequences for exons 1 and 2, respectively, 3 sequences from each exon were selected for cloning (Table 4.3). These guide sequences listed were used to create the sgRNA-top and sgRNA-bottom sequences by adding CACCG adapter at the 5' end of the listed sequence, and adding AAAC at the 5' end of the reverse complement.

Table 4.3. Guide sequences selected for cloning (Numbers: their position on the submitted sequence; fw or rev: their direction on the gene).

Exon	ID	Sequence (5'-3')
1	144rev	TAGGGAGGATCGCCGCACCG
	167fw	CGGTGCGGCGATCCTCCCTA
	294fw	CGGCTTAGGCTTCGTGCCGG
2	258rev	TATACCTGTCAACCGTTAAG
	274fw	CGGTCCCCTTAACGGTTGAC
	782fw	CAGCAAGCGCTTCCGTACCA

Their respective complementary sequences were generated, and adapter sequences required for cloning were added. Resulting oligonucleotides were purchased from Macrogen Inc. (Korea).

4.2.2. Cloning Guide Sequences into px458 Plasmid

Cloning was carried out following protocol published by by Ran, et al. (2014) [42]. Purchased sgRNA oligos and their complimentary sequences were first annealed using the reagents and amounts outlined in Table 4.4.

The reaction mixture is incubated in thermal cycler at 95^0C for 5 minutes followed by reducing the temperature by 5^0C per minute down to target temperature of 25^0C. Annealed oligomer solution was then diluted 1:200 by adding 1 µl of annealed oligomer solution to 199 µl ddH_2O.

Table 4.4. sgRNA oligo annealing reaction mixture.

Reagent	Amount
sgRNA top (100 μM)	1 μl
sgRNA bottom (100 μM)	1 μl
10X T4 ligation buffer (Promega)	1 μl
ddH_2O	7 μl

Annealed sgRNA oligomers were then cloned into px458 plasmid using the reaction mixture in Table 4.5.

Table 4.5. sgRNA cloning reaction mixture.

Reagent	Amount
px458 plasmid	100 ng
Diluted sgRNA duplex	2 μl
10X Tango buffer (Thermo Sci.)	2 μl
DTT (10 mM)	1 μl
ATP (10 mM)	1 μl
Fast Digest BpiI (Thermo Sci.)	1 μł
T4 ligase (Promega)	0.5 μł
ddH_2O	up to 20 μl

Final mixture was incubated in the thermal cycler for 6 cycles of 37^0C for 5 min. followed by 21^0C for 5 min. Obtained plasmids were transformed and isolated as described above.

4.2.3. In-vitro Verification of Plasmids

Obtained constructs were checked for insertion using custom designed primer sets (Table 4.7).

Table 4.6. Obtained CRISPR/Cas9 constructs.

Plasmid backbone	Insert	Cas9 type	Reporter
px458	258rev	Endonuclease	GFP
	274fw	Endonuclease	GFP
	294fw	Endonuclease	GFP

Table 4.7. Primers used for insert check in px458 plasmid.

Primer	Sequence (5'-3')
sgRNAcheckF	GGCCTATTTCCCATGATTCCT
sgRNAcheckR	CGACTCGGTGCCACTTTT
BbsI_siteF	ACGAAACACCGGGTCTTC

These primers were designed to produce a band pattern that is used to determine weather the plasmid contains the sgRNA construct or not. BbsI, a type IIS restriction enzyme, cuts the plasmid twice at positions 246 and 268 to produce the overhangs used in the sgRNA cloning. After a successful digestion reaction followed by successful ligation of the sgRNA sequence, BbsI recognition sites are removed from the plasmid using the advantage the BbsI restriction enzyme's type. Therefore, using a primer that aligns to this stretch of sequence can be used to determine if the cloning is successful. sgRNAcheckF primer should always produce a band if the colony contains the px458 plasmid.

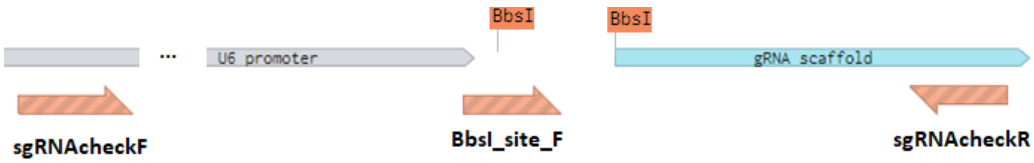

Figure 4.1. PCR design for sgRNA insert check in px458 plasmid.

The expected base pairs and band patterns are outlined in Table 4.8. Colonies positive for insert and negative for the BbsI site according to the PCR band patterns were used for plasmid miniprep. Obtained plasmids were confirmed for insertion using Sanger sequencing using human U6 Forward universal primer.

Table 4.8. Expected band patterns under different cloning outcomes.

Forward Primer	Expected Size	Doesn't Contain Plasmid	Contains Plasmid & No Insert	Contains Plasmid & Contains Insert
sgRNAcheckF	336 bps	-	+	+
BbsI_siteF	100 bps	-	+	-

4.3. Bioinformatic Analysis of GPR139

4.3.1. Analysis of Gpr139 Transcript Levels in Embryonic Mouse Brain

Total RNAseq data submitted by Barbara Wold's group to the ENCODE [40] for mouse forebrain, midbrain and hindbrain were examined to assess the levels of *Gpr139* transcripts in different stages of embryonic development. Datasets used in this analysis are listed in Table 4.9. Each dataset contained RNAseq results from a pooled sample of mixed sex embryo brains at indicated days. Each dataset included two biological samples and technical duplicates from each biological sample.

Following processes and analysis were done with in-house written Ptyhon scripts. File metadata was downloaded, and tab separated values (.tsv) files containing gene quantifications of each biological sample were. From each file, the line corresponding to Gpr139 (ENSMUSG00000066197) was found and TPM value, 95% confidence intervals and embryonic stage values were extracted. Values corresponding to the same stage from both biological samples were combined and the average value of TPMs is calculated. Resulting information were written to a new file for each section and embryonic day. Same process was repeated to obtain values for control genes.

Obtained data was exported to Microsoft Excel and plotted. Expression levels were compared against previous day using 2-way ANOVA to detect significant changes between developmental time points.

Table 4.9. ENCODE IDs of datasets used in RNAseq analysis

Day	Forebrain	Midbrain	Hindbrain
E10.5	ENCSR304RDL	ENCSR764OPZ	ENCSR943LKA
E11.5	ENCSR160IIN	ENCSR307BCA	ENCSR760TOE
E12.5	ENCSR647QBV	ENCSR908JWT	ENCSR420QTO
E13.5	ENCSR970EWM	ENCSR792RJV	ENCSR921PRX
E14.5	ENCSR185LWM	ENCSR343YLB	ENCSR559TRB
E15.5	ENCSR752RGN	ENCSR557RMA	ENCSR401BSG
E16.5	ENCSR080EVZ	ENCSR367ZPZ	ENCSR285WZV
P0	ENCSR362AIZ	ENCSR719NAJ	ENCSR017JEG

4.3.2. Analysis of DNA Methylation of Gpr139 in Embryonic Mouse Brain

Whole genome bisulfite sequencing (WGBS) data submitted by Ecker group was obtained from ENCODE Project (Table 4.10). Data had the same structure as the RNAseq data mentioned earlier (mixed sex embryonic brain, 2 biological samples, 2 technical replicates from each sample). Following processes were done using in-house written Python scripts. From each dataset, bedMethyl files containing methylation states at CpG were downloaded for each biological sample. Intersections of biological samples in *Gpr139* locus were obtained for each bedMethyl file and written to a new .bed file. Lines corresponding to *Gpr139*'s regulatory region (CDS start – 3000 : CDS start), predicted promoter region, 5' CTCF region and the CpG island covering most of exon1, whole 5'UTR and 153 bases 5' upstream of the gene were extracted and average methylation values were calculated.

Table 4.10. ENCODE IDs of datasets used in WGBS analysis.

Day	Forebrain	Midbrain	Hindbrain
E10.5	ENCSR888JFA	ENCSR803ICQ	ENCSR324XQF
E11.5	ENCSR271HQP	ENCSR091VFX	ENCSR398UCM
E12.5	ENCSR007JSP	ENCSR634OPL	ENCSR609ZCD
E13.5	ENCSR141ZVB	ENCSR952CMN	ENCSR734GST
E14.5	ENCSR415FAF	ENCSR344GSM	ENCSR804EWT
E15.5	ENCSR019HJV	ENCSR634OPL	ENCSR227RPE
E16.5	ENCSR430SAY	ENCSR871FJZ	ENCSR037RNN
P0	ENCSR020GGM	ENCSR874LLF	ENCSR168RTO

4.3.3. Analysis of Histone ChiP-seq Data of Gpr139 in Embryonic Mouse Brain

ChiP-seq data submitted by Ren group for E10.5, E11.5, E12.5, E13.5, E14.5, E15.5, E16.5 and P0 for H3K4me3, H3K4me1, H3K9me3, H3K36me3, H3K27me3, H3K4me2, H3K9ac and H3K27ac for fore, mid and hindbrain sections were used for this analysis. Bed narrowPeak files downloaded from ENCODE. From each file, any peaks that falls within the boundary of Gpr139 gene in the mouse genome (plus 5000 bases up and downstream of 5' and 3' UTRs, respectively) were filtered. These peaks were then plotted using Matplotlib module in Python.

4.4. Knock-out Mice Experiments

All animal experiments were done with permission from Bogazici University Institutional Ethics Committee for the Local Use of Animals in Experiments (28.12.17-2017/5). Generation of Gpr139 knock-out mouse model are done in collaboration with Istanbul University Faculty of Veterinary Sciences Department of Reproduction and Artificial Insemination (IU RAI).

4.4.1. In vitro mRNA Synthesis

Previously described protocol was followed for in-vitro transcription of Cas9 mRNA and sgRNA 274 [42]. For sgRNA 274 and Cas9 mRNA synthesis, px458-274 construct and px330 plasmid were used, respectively. Briefly, T7 promoter sequences were added to both sgRNA 274 scaffold and Cas9 CDS via PCR by using primers containing the T7 promoter sequence. Resulting PCR products were then gel-extracted and used as template for in-vitro transcription using MEGAshortscript T7 and mMESSAGE mMACHINE T7 ultra kits for sgRNA 274 and Cas9 mRNA, respectively

4.4.2. Preparation of Mice

4.4.2.1. Preparation of Vasectomized Male Mice. BALB\C males with previous successful insemination history were vasectomized following general procedures. Briefly, an incision was made in the abdomen and testes were taken out of the incision. Vas deferens were cauterized from two separate places and the tissue in between was taken out. Peritoneum and muscle tissue were stitched separately. Animals were reconstituted and checked for signs of infection and/or discomfort. Vasectomized males were subjected to two insemination trials. All vasectomized males successfully plugged females and did not impregnate the females. These mice were used for production of pseudo-pregnant surrogate mothers

4.4.2.2. Preparation of Embryo Donors. For embryo collection, CB6 hybrid mouse were produced by crossing male C56BL/6 with female BALB/C mice. Hybrids were chosen as embryo donors due to their increased embryo production and reduced chance of 2 cell stage arrest during in-vitro cultivation. Obtained females were used as embryo donors, and males were used as studs.

4.4.2.3. Hyper-ovulation and Embryo Collection. Prepared female CB6 hybrids were injected with 7.5 IU of pregnant mare serum gonadotropin (PMSG) at 14:00 on day 1, 7.5 IU of human chorionic gonadotropin (hCG) at 14:00 on day 3.

The injected mice were immediately placed with studs that were housed alone for at least 2 days. Next morning (day 4) at 7:00, females with plugs were identified and transported to Istanbul University. At 10:00, females were sacrificed by cervical dislocation and their ampullas were isolated. Embryos were collected from ampullas and treated with hyaluronidase in M2 medium (300 μg/ml) for at least 5 minutes. Embryos were then washed in M2 medium w/o hyaluronidase and transferred to M16 medium droplets under mineral oil and incubated at 37^0C in 5% CO_2 incubator until injection.

4.4.3. Microinjection of RNA Into Mice Embryo

Microinjection experiments were performed immediately after embryo collection. Injection mixture (Cas9 (100 ng/μl) + sgRNA (50 ng/μl)) was prepared and volume was brought to 5 μl using nuclease free water. In a 10 cm cell culture grade dish, droplets for injection mix (5 μl) and M2 medium were prepared under mineral oil. Batches of isolated embryo were transferred to the M2 medium for injection.

Injection and suction pipettes were hand-drawn. Injection pipette was primed with 2-to-3 mm of mercury (Hg) using a syringe with 26G needle. The pipette was then attached to the piezzo pulse unit and the assembly was attached to the micro-manupilator. Mercury droplet was moved to the end of the injection pipette and washed in PVP solution. Injection mix was aspirated after priming and washing the injection pipette.

Zygotes were held using the aspiration pipette and a few piezzo pulses at power level 4 and duration 4 to break the zona pellicuda. Pipette tip was moved forward without breaking the oolemma until almost reaching the opposite site of the cortex. One weak piezzo pulse was applied to break the oolemma. With the pipette inside the zygote's cytoplasm, 2 pl of the injection mixture was injected and pipette was immediately pulled out.

Injected embryos were transferred to M16 medium droplets under mineral oil and incubated at 37^0C in 5% CO_2 incubator until observation.

4.4.4. Embryo Culture and Selection

Injected embryo were incubated at 37^0C in 5% CO_2 in M16 medium previously equilibrated for at least 30 minutes in the incubator. After 24 and 72 hours embryos were checked for 2-cell and blastocyst stages, respectively. Two cell embryos were used for oviduct transfer and blastocyst stage embryos were used for uterus transfer.

4.4.5. In-vitro Verification of Gpr139 Deletion

Injected embryos were observed for 72 hours for any morphological abnormalities. After 72 hours, single embryos with normal morphology were transferred to the bottom 0.2 ml tubes submerged in liquid nitrogen and flash frozen. 10 µl of blastocyst lysis buffer (Table 4.11) was added to the tube. Tubes were then incubated at 56C for 1 hour followed by 95^{o}C for 10 minutes. Prepared lysates were either stored at -80^{o}C or immediately used for PCR reaction (Table 4.12).

Table 4.11. Blastocyst Lysis Buffer

Ingredient	Final Concentration
Proteinase K	200 µg/ml
Tris.Cl ph 8.3	100 mM
KCl	100 mM
Tween 20	0.45%
Gelatin	0.02%

The PCR reaction was performed as described in Section 4.1.3 using 63^{o}C as initial annealing temperature, -1^{o}C/cycle for 10 cycles and 30 cycles at the final annealing temperature. Samples were than loaded on 1% agarose gel for visualization.

Table 4.12. Reaction mixture for blastocyst PCR

Ingredient	Amount (µl)
Mytaq buffer (5X)	5
Primer mix	0.5
Template	2
Mytaq polymerase	0.2
Water	17.3

4.4.5.1. Preparation of Pseudo-pregnant Surrogate Females. Female CD1 mice were used as surrogate mothers. Six to eight week old virgin CD1 female mice were housed with vasectomized male mice in the morning of embryo transfer. Plug formation was checked the next day immediately after the start of the light cycle. Females with visible plugs were selected as surrogate mothers.

4.4.6. Transferring Injected Embryo to Surrogate Mice

Following *in vitro* cultivation, embryos without morphological anomalies were transferred to surrogate mothers. Plugged surrogate females were anesthetized via 0.25% (v/v) tribromoethanol (0.015 ml/g) injection into the peritoneal cavity. Anaesthesia was checked by pinching the hind feet. While the mice are under anaesthesia, mice were placed on the operation table and their backs were shaved and sterilized with betadine (10%) followed by ethanol (70% v/v). A small incision between 0.5 to 1 cm is made above the ovary. After the skin incision, the ovary was located under the muscle membrane and the membrane is cut using scissors. The ovary was gently taken out of the body cavity by attaching small clamps to the fat pad. Infundibulum was located and bursa covering the targeted sections was gently pierced and moved away using forceps. Using a mouse pipette, 15 to 25 embryos were transferred into the infundibulum towards the oviduct. After the transfer, the ovary was replaced into the body cavity and the muscle membrane is sutured. Skin was either sutured, stapled or glued using 2-octyl cyanoacrylate. Carprofen (5 mg/kg) diluted in 300 µl isotonic saline solution was injected subdermally for pain relief.

Operated mice were transferred to their cages and observed until they gained normal mobility. Mice were checked daily for normal behavior, and intactness and healing progress of the incision.

4.5. GPCR139 Ablation in Adult Mice

All animal experiments for ablation studies were done with permission from İstanbul Medipol Üniversitesi Hayvan Deneyleri Yerel Etik Kurul Başkanlığı (permission no 38828720-604.01.01-E.32272).

4.5.1. Plasmid Preparation

AAV-U6-sgRNA-hSyn-mCherry (px552mcherry was a gift from Alex Hewitt (Addgene plasmid 87916) [45]. sgRNA constructs 274 and 294 were cloned into px552mcherry plasmids as described in Section 4.2.2 to obtain AAV-274 and AAV-294 constructs, respectively.

4.5.2. Cell Culture Experiments

For adenoassociated virus (AAV) preparation, HEK293FT cells were used. The day before transfection, $10x10^7$ cells were seeded on ten 15 cm cell culture dishes using DMEM culture medium containing 2% fetal bovine serum (FBS) and 1X penicillin/streptomycin. When cells reach 70-to-80% confluency, transfection was carried out.

4.5.2.1. Transfection. Transfection was carried out using polyethylenimine (PEI) protocol. Trnasfection mixture was prepared per plate by adding 120 μg helper and 100 μg 2/1 plasmids in 0.5 ml DMEM, vortexing for 10 seconds, adding 30 μg of AAV-294 and AAV-274 each for the experiment group or 60 μg AAV-control plasmid control group, vortexing an additional 15 seconds, adding 0.5 ml of 1 mg/ml PEI solution, vortexing for 10 seconds and incubating at room temperature for 10 minutes.

Resulting solution was added drop-wise, 1 ml to each plate. The transfection mixture was scaled up as needed.

Cells were checked for mCherry signal using fluorescent microscope. Transfected cells were incubated for 72 hours and harvested by scraping the cells without removing the media, transferring to 50 ml centrifuge tubes, centrifuging at 200g for 5 minutes at room temperature and aspirating the supernatant. Cell pellets were stored at -80^{o}C until AAV isolation.

4.5.3. AAV Isolation

Frozen cell pellets were thawed and re-spun at 4500g for 10 minutes at room temperature. Remaining supernatant was removed and cells containing the same constructs were combined by resuspending the pellets with 9 ml lysis buffer (150 mM NaCl, 20 mM Tris pH 8.0), resuspending the pellet and transferring the suspension to the next tube until all cells are collected in the last tube. Final suspension was then transferred to a 15 ml centrifuge tube. Tubes were then subjected to 3 freeze and thaw cycles by placing the tubes in -80^{o}C until frozen and 37^{o}C water bath until completely thawed for each cycle. After final thawing step, cells are sonicated for 15 seconds in ultrasonic bath sonicator with 50% on cycle for 15 seconds. Benzonase was added to a final concentration of 250 U/ml and mixed. Tubes were incubated 45 minutes at 37^{o}C in a water bath and spun at 3000 g for 20 minutes at 4^{o}C. Using a syringe and 18G needle, 8 ml 17%, 6 ml 25%, 5 ml 40% and 5 ml 60% iodixanol solutions (Table 4.13) used to create layers in a QuickSeal ultrafuge tube. After the incubation, cell lysate containing the AAVs is layered on top of the 17% iodixanol layer. Remaining volume in the ultrafuge tube, if any, was filled using lysis buffer. Tubes are then sealed and spun at 230K g for 2 hours at 18^{o}C.

AAV virus particles are expected to settle at the 40% layer after the centrifuge. To collect the AAV virus particles, a hypodermic needle was inserted at the 60% - 40% interface with the bevel of the needle facing the 40% layer. Forty per cent layer was collected as much as possible without aspirating any of the 25% layer.

Table 4.13. Iodixanol solutions used in AAV isolation

	60%	40%	25%	17%
10X PBS	5 ml	5 ml	5 ml	5 ml
1M MgCl2	0.05 ml	0.05 ml	0.05 ml	0.05 ml
1M KCl	0.125 ml	0.125 ml	0.125 ml	0.125 ml
5M Nacl	10 ml	10 ml	10 ml	10 ml
Optiprep	50 ml	33.3 ml	20 ml	12.5 ml
0.5% phenol red	0.025 ml	-	0.1 ml	-
ddH2O	-	up to 50 ml	up to 50 ml	up to 50 ml

Millipore Amicon 100K filters were wetted using 2 ml AAV storage buffer (Table 4.14). Collected AAV virus particle fractions were mixed with 11 ml AAV storage buffer to dilute iodixanol and added to the filter reservoirs. Filters were then spun at 3660 g for 25 minutes at room temperature and flow through was discarded. Fresh 15 ml storage buffer was added to the reservoir and mixed by pipetting up and down to reconstitute the iodixanol settled on the membrane. Filters were then spun again at 3660 g for 30 minutes at room temperature and flow through was discarded. This wash step is performed once more to wash iodixanol completely. The total volume in the reservoir was brought up to 500 µl using the volume marks on the reservoir wall using AAV storage buffer. The membrane was then washed several times using the liquid in the reservoir to resuspend the virus particles settled on the membrane. Obtained solution was then transferred to a 1.5 ml microfuge tube and stored at 4^oC until quantification.

AAV-cre virus used in this study was prepared using AAV-GFP/Cre plasmid (Addgene plasmid 49056) [46] kindly provided by Asst. Prof. Deniz Atasoy.

4.5.4. AAV Titration

A mini prep solution of AAV-274 plasmid was used to create the standard curve for AAV titration. As a standard solution, $2x10^9$ molecule/µl solution and its dilutions were prepared (Table 4.15).

Table 4.14. AAV storage buffer composition

Reagent	Amount
10X PBS	100 ml
D-sorbitol	50 g
5M NaCl	42.4 ml

All dilutions except for $2x10^9$ was used to create the normal curve. AAV isolates were first subjected to DNaseI digestion to remove any non-enclosed DNA particles. For DNaseI digestion, 10X DNaseI buffer was prepared (Table 4.16) and the pH was adjusted to 7.6.

Table 4.15. Reference sample dilution scheme for AAV titration.

Particles per µl	Previous dilution (µl)	ddH2O (µl)
$2x10^9$	-	-
10^9	50	50
10^8	10	90
10^7	10	90
10^6	10	90
10^5	10	90
10^4	10	90

The reaction mixture was prepared according to Table 4.17 and incubated at 37^{o}C for 30 minutes. The AAV solution was then diluted according to Table 4.20. Dilutions with dilution factor between 5000X and 625000X were used for titration.

Table 4.16. 10X DNaseI buffer composition.

Reagent	Final Concentration
Tris.Cl	100 mM
$MgCl_2$	25 mM
$CaCl_2$	5 mM

Table 4.17. DNaseI digestion reaction composition.

Ingredient	Volume (µl)
AAV stock	5
ddH_2O	39
10X DNaseI buffer	5
DNaseI (2500 U/ml)	1

AAV titration was performed using qPCR. Reference samples and AAV solutions were used in duplicates. The reaction was prepared according to Table 4.18.

Reaction mixtures were transferred to 96 well opaque white plates, sealed with transparent film and spun at 200 g for 30 seconds. Plates were then loaded to LightCycler 480 (Roche, Switzerland) and the reaction was run following the protocol outlined in Table 4.19. At the end of each cycle the fluorescence values were read. Melting curve analysis was performed at the thermal cycle.

Data analysis was performed using LightCycler 480 analysis software (Roche, Switzerland) with absolute quantification option. Average values of duplicates were used for calculations. Using the reference sample, the standard curve was plotted and the curve formula was calculated. Ct values of AAV samples were used to calculate the estimated titers of the serial dilution.

Table 4.18. qPCR composition for AAV titration.

Ingredient	Volume (µl)
Universal SYBER Mix (2X)	10
Forward Primer (100 µM)	0.15
Reverse primer (100 µM)	0.15
ddH_2O	4.7
Template	5

Table 4.19. AAV titration qPCR thermal cycler program.

Temperature	Duration	Cycles
98^oC	3 min	1
98^oC 58^oC	15 sec 30 sec	39

Primer efficiency was calculated as $Efficiency(\%) = 100(10^{\frac{-1}{slope}} - 1)$

4.5.5. In Vitro and In Vivo Confirmation of AAVs

Prepared AAV solution was used to transduce primary mouse neuron culture cells kindly provided by Asst. Prof. Muhammed İkbal Alp. One week after transduction, cells were visualized under fluorescent microscope for mCherry signal.

Table 4.20. Sample dilution chart for AAV titration.

Dilution Factor	Volume of sample (µl)	ddH_2O (µl)
10X	5 of stock	45
200X	5 of 10X	95
1000X	20 of 200X	80
5000X	20 of 1000X	80
25000X	20 of 5000X	80
125000X	20 of 25000X	80
625000X	20 of 125000X	80

4.5.6. Intracranial Injection Experiments

Four to six week old male Rosa26-floxed STOP-Cas9 knock-in mice (Jax strain number: 024857) were used for intracranial injection experiments. Mice were anesthetized using isoflurane inhalation and placed in the stereotaxic frame. Their skulls were fixed using ear bars. After re-confirming that the mice are still under anaesthesia, their heads were shaved and sterilized using betadine solution. Using a sharp scalpel, incision was made on their scalps revealing the skull. Hydrogen peroxide solution was used to remove the periost and bleach the skull for easier observation. The hydrogen peroxide solution was then rinsed. Using SteREO Discovery V8 microscope and digital read out system, digital read out coordinates were zeroed by positioning the probe over the bregma. Probe was then moved to lambda to check if the skull is level in rostral-caudal direction. If needed, the positioning of the head was adjusted by re-adjusting the nose bar. Horizontal positioning of the skull was checked, as well, by moving the probe to the approximate middle of the mid-line and moving the probe on the X axis the same amount on + and - directions and checking the Z heights. If required, horizontal positioning is adjusted by re-adjusting the ear bars.

After confirming the positioning of the skull in the stereotaxic frame, the probe was moved to the injection coordinates y = -1.55 mm, x = ±0.3 mm and the positions were marked on the skull. Two bilateral holes were drilled using a hand-held drill. Bone fragments were carefully washed using 1X PBS solution.

The probe was changed with the injection needle previously filled with mineral oil. Injection solution (AAV-274:AAV-294:AAV-cre, 1:1:2) was then aspirated into the needle and the needle was positioned over the bregma to re-zero the coordinates. Needle was then moved to the injection coordinates and descended slowly until reaching the brain surface. Z coordinate was zeroed and the needle was slowly inserted into the brain matter at the rate of 1 mm/min until reaching -3.00 mm. Injection was performed at the rate of 75 nl/min until 300 nl of the AAV solution was discharged. Needle was kept in place for 10 minutes to allow time for the injection solution to diffuse. It was then carefully removed at the rate of 1 mm/min. The scalp was then sutured and the mice were transferred to resuscitation chamber. After resuscitation, mice were transferred to their home cages. They were observed for 21 days after the operation for visible unwanted effects such as seizures, immobility as well as healing process. This time period also allowed for the AAV expression.

4.6. Animal Behavioral Experiments

4.6.1. Morris Water Maze

Morris water maze is used as a measure of spatial learning. For this test, opaque black water tank with 120 cm diameter was used. The water tank was filled with tap water and heated to 22^{o}C. Food grade lithium dioxide dye was used to color the water opaque white. The tank was divided into 8 sections and the white hidden platform was placed in the NE section 1 cm below the water level. Mice were brought to the preparation area near the test chamber. When performing the experiment, mice were gently removed from their cages and lowered into the water maze following the start positions outlined in Table 4.21. Test was performed for 1 minute.

During the test period, if the mice did not find the platform within the test duration, they are guided to the platform or gently put on the platform. The animals were left on the platform for 30 seconds. After the test, mice were removed from the chamber, dried with paper towels and put back into their home cages. The tests were recorded via a CCD camera and results were analyzed using AnyMaze software.

Table 4.21. Morris water maze test start positions according to trial days.

Day	Trial 1	Trial 2	Trial 3	Trial 4
1	N	E	SE	NW
2	SE	N	NW	E
3	NW	SE	E	N
4	E	NW	N	SE
5	N	SE	E	NW

4.6.2. Elevated Plus Maze

Opaque white plastic plus maze was placed 35 cm above the test table. The maze had four arms with 5 cm x 35 cm dimensions. Two of the arms opposite each other had 20 cm opaque walls. Mice were habituated in the test room for 1 hour. After habituation, mice were placed at the center of the maze, facing the open arm. Mice were observed for 5 minutes and replaced in their home cages. The maze was cleaned thoroughly after each test first with water and then with 70% ethanol. Ethanol was allowed to dry completely. The tests were recorded via a CCD camera and results were analyzed using AnyMaze software.

4.6.3. Open Field Test

A white opaque chamber with 40 x 40 x 40 cm dimensions was used for the open field tests. The mice was acclimatized to the test room for 1 day. On the test day, the animals were brought to the test room 1 hour before the start of the first test.

To perform the test, the mice were removed from their home cage and placed in the middle of the test chamber. The tests were completed after 10 minutes and the test chamber was cleaned thoroughly after each test first with water and then with 70% ethanol. Test sessions were recorded via a CCD camera and results were analyzed using AnyMaze software.

4.6.4. Novel Object Recognition Test

These tests were performed using the same chamber used in the open field test. Following the day of the open field test, two familiar objects were placed at opposing corners 5 cm away from the chamber walls. Mice were placed gently in the middle of the chamber and monitored for 10 minutes. After 10 minutes, mice were removed and the test chamber as well as the objects were cleaned thoroughly after each test first with water and then with 70% ethanol. The two familiar objects were replaced with an identical object and a novel object, and the test procedure was repeated. Test sessions were recorded via a CCD camera and results were analyzed using AnyMaze software. Discrimination ratio between the novel and fixed objects is calculated as $DR = \frac{T_{novel} - T_{fixed}}{T_{total}}$

5. RESULTS

5.1. Gpr139 Has Differential Expression in Embryonic Mouse Brain

Total RNAseq data submitted by Barbara Wold's group for mouse forebrain, midbrain and hindbrain were examined to assess the levels of Gpr139 transcripts in different stages of embryonic development. Each dataset contained RNAseq results from a pooled sample of mixed-sex embryo brains at indicated days and two biological samples and technical duplicates from each biological sample. Following processes and analysis were done with in-house written Python scripts. File metadata was downloaded and tab separated values (.tsv) files containing gene quantifications of each biological sample were obtained using the information provided in the metadata file. From each file, the line corresponding to Gpr139 (ENSMUSG00000066197) was found and TPM value, 95% confidence intervals and embryonic stage values were extracted. Values corresponding to the same stage from both biological samples were combined and the average value of TPMs is calculated. Resulting information were written to a new file for each section and embryonic day. Same process was repeated to obtain values for control genes.

Rhodopsin and frizzled 7 GPCRs were included in this analysis as negative and positive controls, respectively. Transcript per million (TPM) values for rhodopsin fluctuated between 0.025 and 0.115 whereas those for frizzled 7 were between 1.43 and 8.04 in forebrain and 1.34 and 15.75 in hind and mid brains with higher expression values in E10.5, E11.5 and E12.5 and reduced expression from E13.5. Gpr139 TPM values steadily increased in all three brain sections between E10.5 to E14.5 and kept a high level in E15.5, E16.5 and P0 (Figure 5.1).

In a larger scale analysis, higher levels of TPM values of Gpr139 was observed in the central nervous system including whole brain, frontal cortex, neural tube, central nervous system and cerebellum data sets while the expression levels remained close to 0 in the rest of the data sets (Figure 5.2).

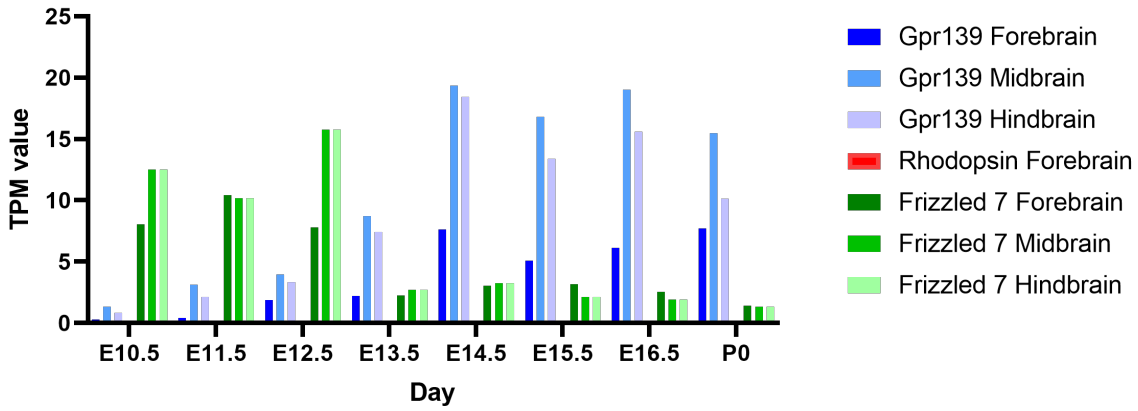

Figure 5.1. TPM values for indicated genes in different embryonic days in mouse brain.

Comparing the TPM values in fore, mid and hindbrain data sets for Gpr139 revealed statistically significant changes in expression levels between embryonic days especially after E12.5 (Table 5.1).

Table 5.1. Student's t-test p values in fore, mid and hindbrain data sets for Gpr139 comparing consecutive embryonic days.

Tissue	Forebrain	Midbrain	Hindbrain
E10.5 vs. E11.5	>0.9999	0.0516	0.1124
E11.5 vs. E12.5	0.0656	0.9972	0.815
E12.5 vs. E13.5	>0.9999	<0.0001	<0.0001
E13.5 vs. E14.5	<0.0001	<0.0001	<0.0001
E14.5 vs. E15.5	0.4537	0.0012	<0.0001
E15.5 vs. E16.5	0.7201	0.0132	<0.0001
E16.5 vs. P0	<0.0001	<0.0001	<0.0001

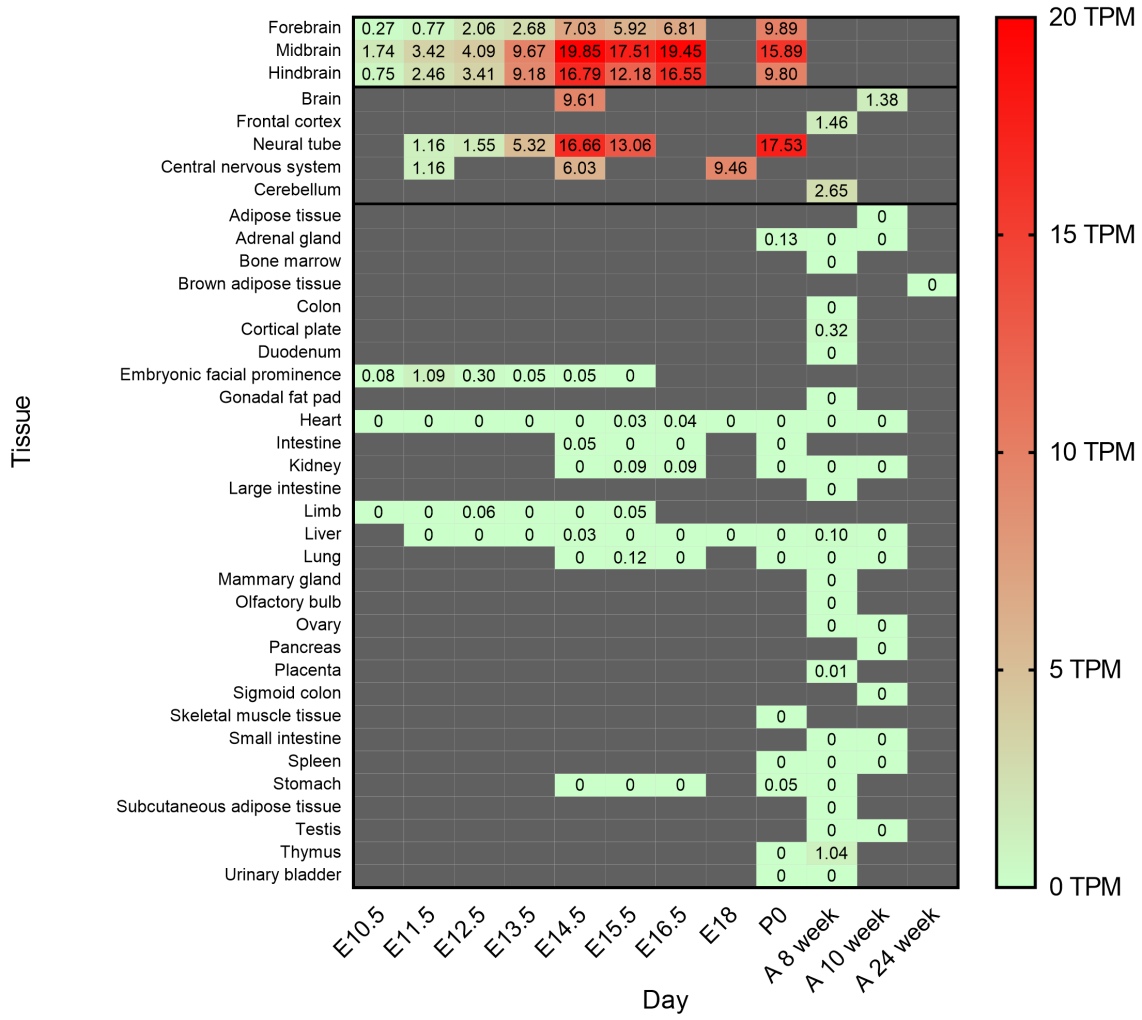

Figure 5.2. Heatmap showing transcript levels of Gpr139 in various tissues and developmental stages (TPM: transcript per million; absent data is shown in gray).

5.1.1. Differential Expression of Gpr139 is not Mediated by DNA Methylation

DNA methylation patterns for fore, mid and hindbrain data sets were used to determine any possible differences in CpG methylation between embryonic days in each data set. Liver data set was used as a negative control. Two distinct methylation islands are observed between bases -5000 to -2500 and -1750 to -1400 in all four data sets included in the analysis with lower levels of methylation in the liver data set compared to fore, mid and hindbrain sections (Figure 5.3).

No significant differences in DNA methylation between different embryonic days in each brain section were observed that could explain the differences in TPM values.

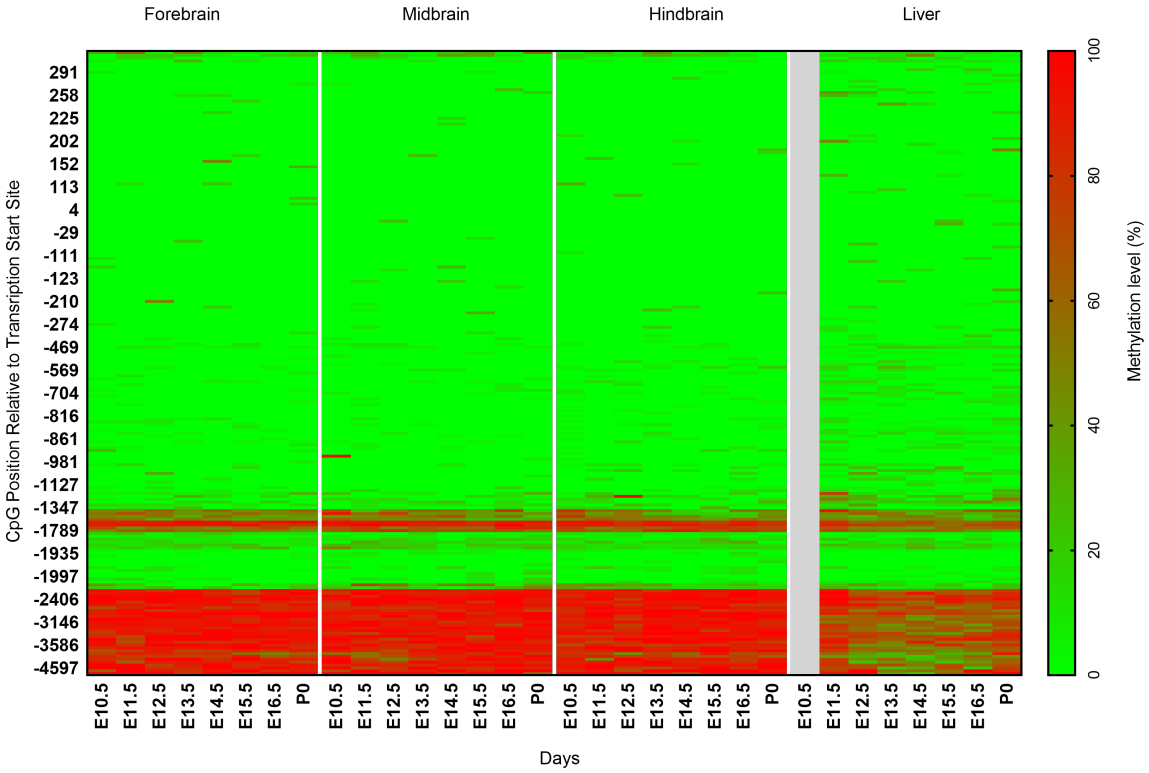

Figure 5.3. Methylation patterns of mouse forebrain, midbrain, hindbrain and liver tissue.

5.1.2. Histone Modifications Explain Differential Expression of Gpr139

Histone modifications were analyzed as potential regulatory mechanism controlling Gpr139 expression. For this analysis, H3K4me2, H3K4me3, H3K9Ac, H3K27Ac and H3K27me3 data sets for hind, fore and midbrain sections were used. Liver data set was included as a negative control. In brain sections, H3K4me2 and H3K4me3 were observed throughout the available embryonic days included in the data set at more or less the same levels while they were absent in the liver sample (Figure 5.4).

H3K9Ac was observed in all three brain sections with increasing levels through the development with the exception of P0, which had reduced levels compared to E16.5. H3K9Ac levels were minimal in the liver sample. H3K27Ac and H3K27me3 levels changed opposite to each other with increasing levels of H3K27Ac and decreasing levels of H3K27me3. H3K27Ac levels were minimal in the liver sample whereas H3K27me3 was observed throughout the available data.

5.2. Knock-out Mice Experiments

5.2.1. In vitro mRNA Synthesis

sgRNA 274 and Cas9 mRNA synthesis was performed using px458-274 construct and px330 plasmid, respectively. For the synthesis, T7 promoter sequences were added to both sgRNA 274 scaffold and Cas9 CDS via PCR by using primers containing the promoter sequence. Resulting PCR products were then gel-extracted and used as template for in-vitro transcription using MEGAshortscript T7 and mMESSAGE mMACHINE T7 ultra kits for sgRNA 274 and Cas9 mRNA, respectively. Obtained RNAs were checked in agarose gel for size and degradation (Figure 5.5).

5.3. In-vitro Verification of GPR139 Deletion

Isolated single embryos that were subjected to Cas9 mRNA + sgRNA scaffold microinjection were used for single embryo PCR. Targeted region of the Gpr139 gene of about 500 bps was amplified and either subjected to T7 endonuclease digestion. Expected length of PCR product was 500 bps and dT7 endonuclease digestion products were 200 and 300 bps. All four samples injected with sgRNA construct 274 analyzed with T7 endonuclease assay yielded digestion bands at expected sizes (Figure 5.6) but the quality was poor. Ten more samples were analyzed via Sanger sequencing. All sequenced samples showed deletion pattern at the targeted position (Figure 5.7).

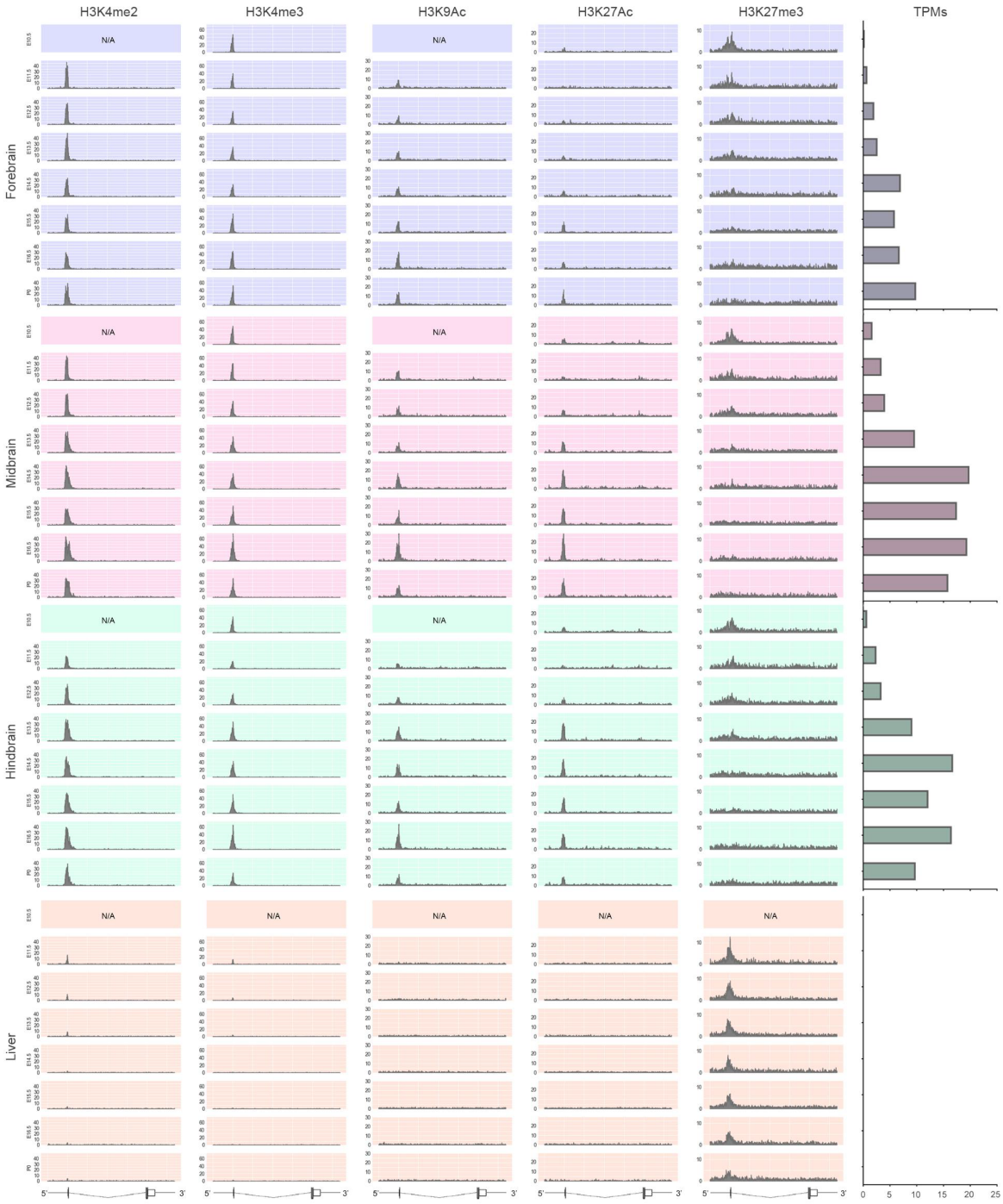

Figure 5.4. Histone modifications on Gpr139 gene in fore-, mid-, hindbrain and liver tissues by embryonic days. Linegraphs show peak values for indicated modification, tissue and time points. Right-most panel shows TPM values for indicated time points. Gene structure is shown at the bottom.

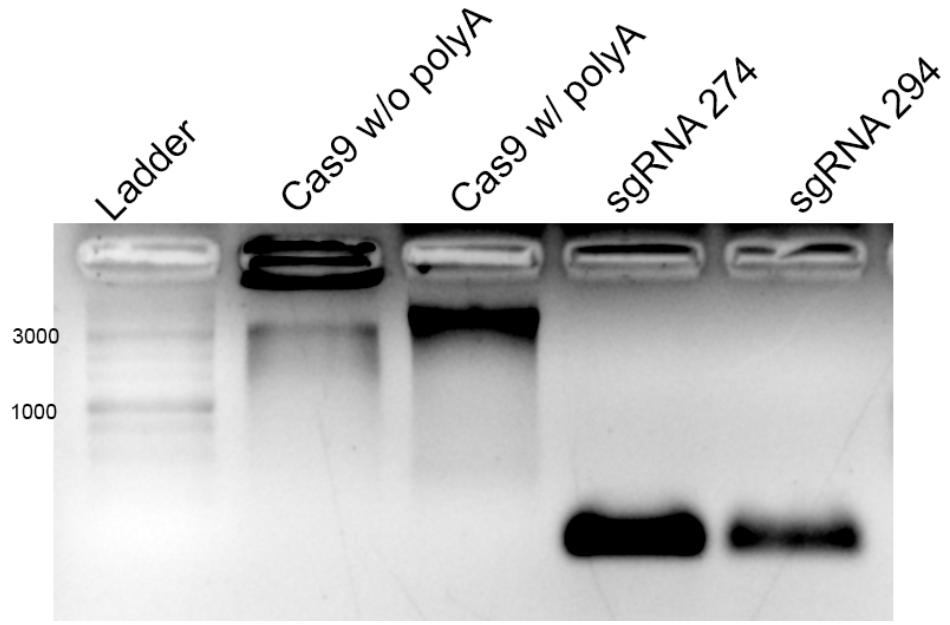

Figure 5.5. Synthesized Cas9 mRNA and sgRNA scaffolds.

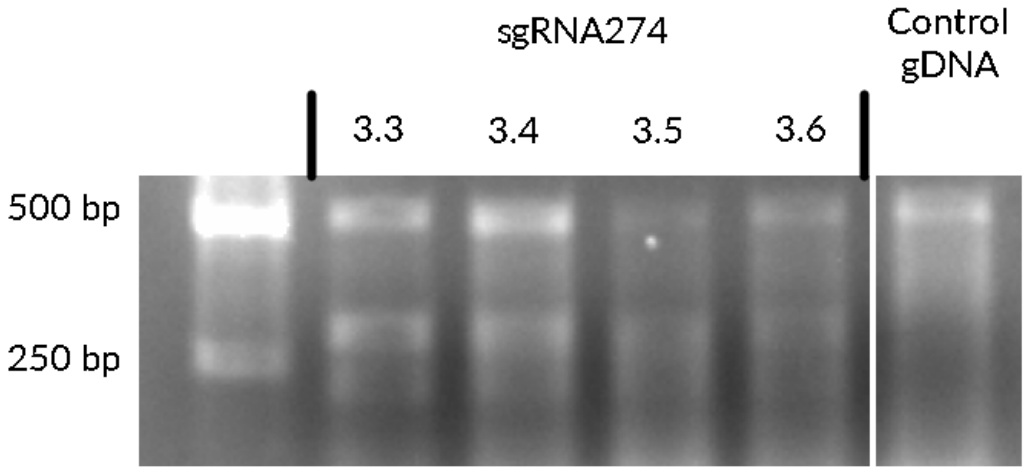

Figure 5.6. T7 endonuclease assay results.

5.3.1. Transferring Injected Embryo to Surrogate Mice

Throughout the study, only successful embryo transfer was obtained with a test group which was only subjected to the same *in-vitro* culture protocol but not subjected to microinjection. Out of the 15 transferred blastocysts, we obtained 5 pups in the control group, 3 of which survived (Figure 5.8).

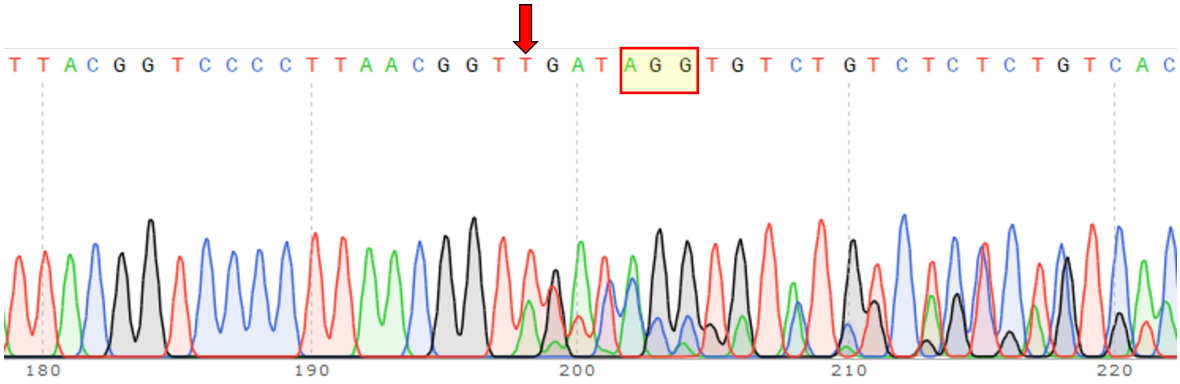

Figure 5.7. Representative chromatogram of the *in-vitro* deletion of Gpr139 in injected embryos. Red arrow indicates the theoretical cut site. Bases outlined with red box are the PAM sequence used in sgRNA scaffold design.

5.4. GPCR139 Ablation in Adult Mice

5.4.1. Adenoassociated Virus Titration

Obtaining exact titration of the AAVs used in experiments is crucial for accuracy and reproducibility of the procedure. There are various steps in AAV production and isolation that can directly affect the concentration of final solutions, which in turn can and will effect the efficacy of experiments. In this study, prepared AAV isolates were titrated by qPCR using dilutions of isolated px458 plasmid with known concentrations as reference (Table 5.2).

Since the AAV titers were calculated using qPCR, primer efficiencies play an important role in accurate quantification. A previously published guideline was followed to design the primers used in this study and calculating their efficiencies [47]. Primer efficiencies for each group of samples were calculated as $Efficiency(\%) = 100(10^{\frac{-1}{slope}} - 1)$ (Table 5.3).

Figure 5.8. Obtained pups (black) and their surrogate mother (white) in the control group of embryo transfer.

5.4.2. In Vitro and In Vivo Confirmation of AAV Solution

One week after transduction, primary mouse cortex cells were visualized under fluorescent microscope for mCherry signal (Figure 5.9).

Intracranial injection protocol and the determined coordinates using Allen Brain Atlas [48] was tested by injecting 300 nl of the AAV solution into y = -1.55 mm, x = ±0.3 mm, z = -3.00 mm. Mice were sacrificed 3 weeks after injection and 50 μm coronal slices were obtained. Slices were visualized under fluorescent microscope for mCherry signal (Figure 5.10).

Table 5.2. Calculated concentrations of standard, AAV and control AAV samples using absolute quantification fit point analysis

Sample	Known Conc. (gc/μl)	Calculated Conc. (gc/μl)
Control 1	$1.00x10^9$	$1.07x10^9$
Control 2	$1.00x10^8$	$8.59x10^7$
Control 3	$1.00x10^7$	$9.39x10^6$
Control 4	$1.00x10^6$	$1.21x10^6$
Control 5	$1.00x10^5$	$1.14x10^5$
Control 6	$1.00x10^4$	$8.60x10^3$
AAV diln. 4	-	$5.56x10^5$
AAV diln. 5	-	$1.99x10^5$
AAV diln. 6	-	$4.73x10^4$
AAV diln. 7	-	$1.26x10^4$
Control AAV diln. 4	-	$1.73x10^6$
Control AAV diln. 5	-	$3.05x10^5$
Control AAV diln. 6	-	$5.77x10^4$
Control AAV diln. 7	-	$1.12x10^4$

Table 5.3. Calculated primer efficiencies for each group of samples used in titration.

Sample Group	Primer Efficiency (%)
Control	97.81
AAV	131.84
Control AAV	89.68

Both *in vitro* and *in vivo* control experiments showed successful transduction and production of the viral plasmid in primary cortex cells, and cells in and near habenula.

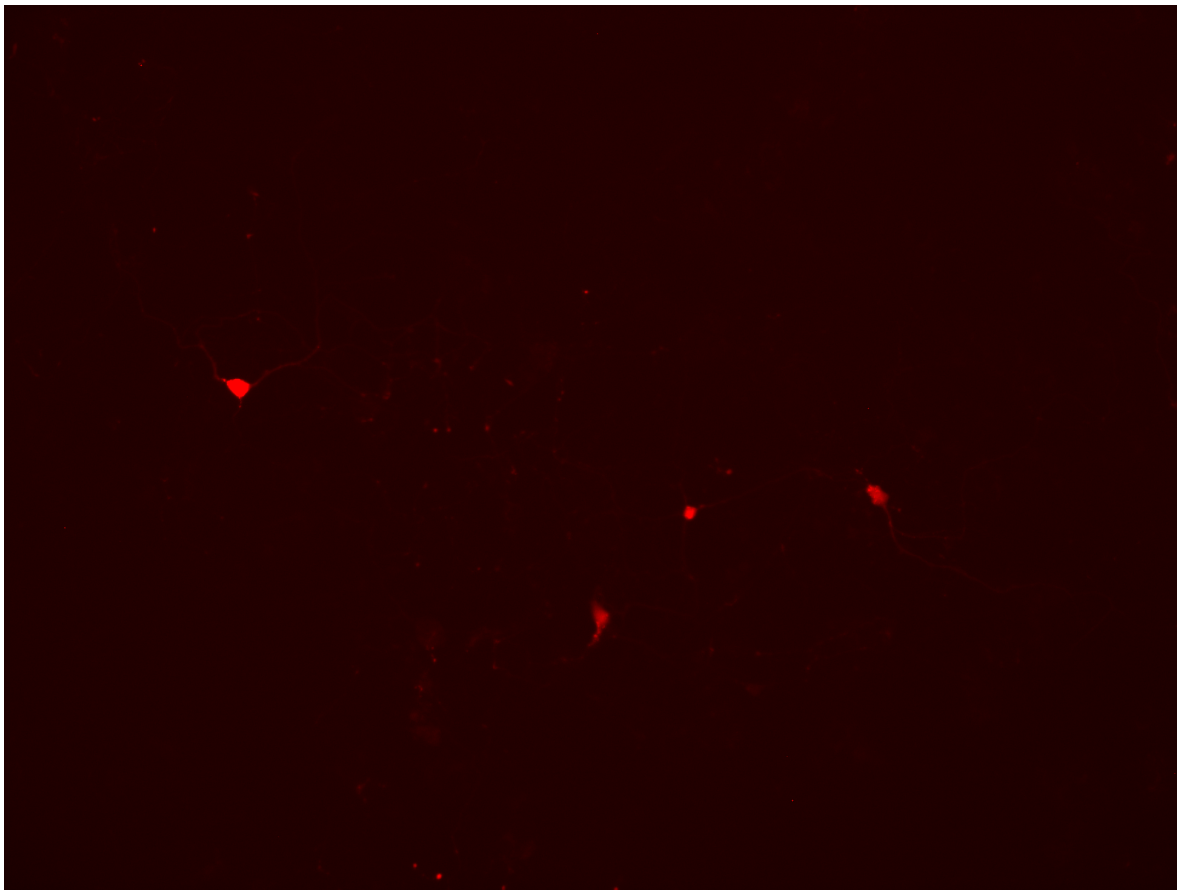

Figure 5.9. mCherry signal in primary mouse cortex cells after transduction with AAV solution.

5.5. Animal Behavioral Experiments

Following intracranial injections and the recovery period, all animals in test and control groups were subjected to behavioral tests to measure the effects of GPR139 ablation, if any, on spatial learning, memory, attention deficiency, mobility and anxiety.

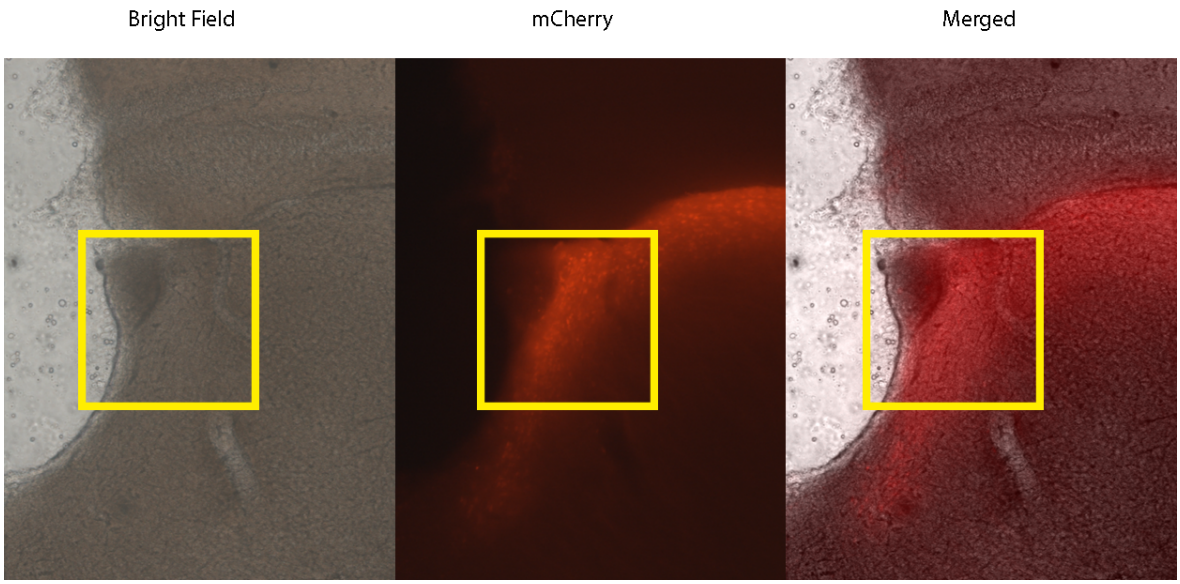

Figure 5.10. AAV injection control in wild type mouse. mCherry (red) shows cells that are transduced and producing sgRNA. Yellow square denotes the relative position of habenula.

5.5.1. Intracranial Injection Experiments

Intracranial injections were performed by injecting 300 nl of the AAV solution to coordinates listed in Table 5.4.

5.5.2. Morris Water Maze

Morris water maze experiment targeted two possible effects of GPR139 ablation: abnormalities in learning and memory, and attention deficiency. As mentioned above, GPR139 has shown to be correlated with ADHD [21] and inattention [22].

Table 5.4. Details of intracranial injections.

ID	λ – Bregma Tilt (mm)	x Axis Tilt (mm)	Injection Coordinates (Relative to Bregma x,y,z; left hemisphere;right hemisphere)
Control 1	0.059	0.065	-0.312,-1.583,-2.842 ; +0.304,-1.583,-2.754
Control 2	0.115	0.020	-0.302,-1.550,-2.759 ; +0.309,-1.551,-2.755
Control 3	0.205	0.101	-0.315,-1.548,-2.748 ; +0.307,-1.547,-2.752
Control 4	0.109	0.196	-0.355,-1.585,-2.847 ; +0.352,-1.585,-2.841
Control 5	0.129	0.103	-0.328,-1.605,-2.798 ; +0.324,-1.604,-2.794
Control 6	0.115	0.020	-0.313,-1.561,-2.749 ; +0.310,-1.561,-2.753
Control 7	0.205	0.101	-0.309,-1.543,-2.816 ; +0.307,-1.547,-2.802
Test 1	0.109	0.196	-0.305,-1.585,-2.847 ; +0.302,-1.585,-2.841
Test 2	0.178	0.098	-0.302,-1.548,-2.728 ; +0.300,-1.548,-2.734
Test 3	0.126	0.201	-0.303,-1.556,-2.735 ; +0.305,-1.556,-2.742
Test 4	0.201	0.171	-0.303,-1.554,-2.754 ; +0.303,-1.554,-2.695
Test 5	0.116	0.012	-0.302,-1.552,-2.694 ; +0.303,-1.552,-2.639
Test 6	0.270	0.150	-0.299,-1.574,-2.624 ; +0.307,-1.576,-2.705
Test 7	0.134	0.052	-0.326,-1.561,-2.712 ; +0.325,1.562,-2.655
Test 8	0.134	0.052	-0.311,-1.568,-2.692 ; +0.305,1.569,-2.714

As can be seen in Figure 5.11, however, there are no significant differences between test and control groups which indicates that the ablation of GPR139 does not affect spatial learning, memory, or any measures that can directly or indirectly affect the performance of mice in morris water maze. Two way ANOVA analysis showed no significant differences between the test and control groups ($p = 0.8415$).

5.5.3. Elevated Plus Maze

Elevated plus maze mainly measures anxiety in rodents. More anxious animals prefer to spend more time in the closed arms while less anxious animals, due to their nature, tend to explore the open arms.

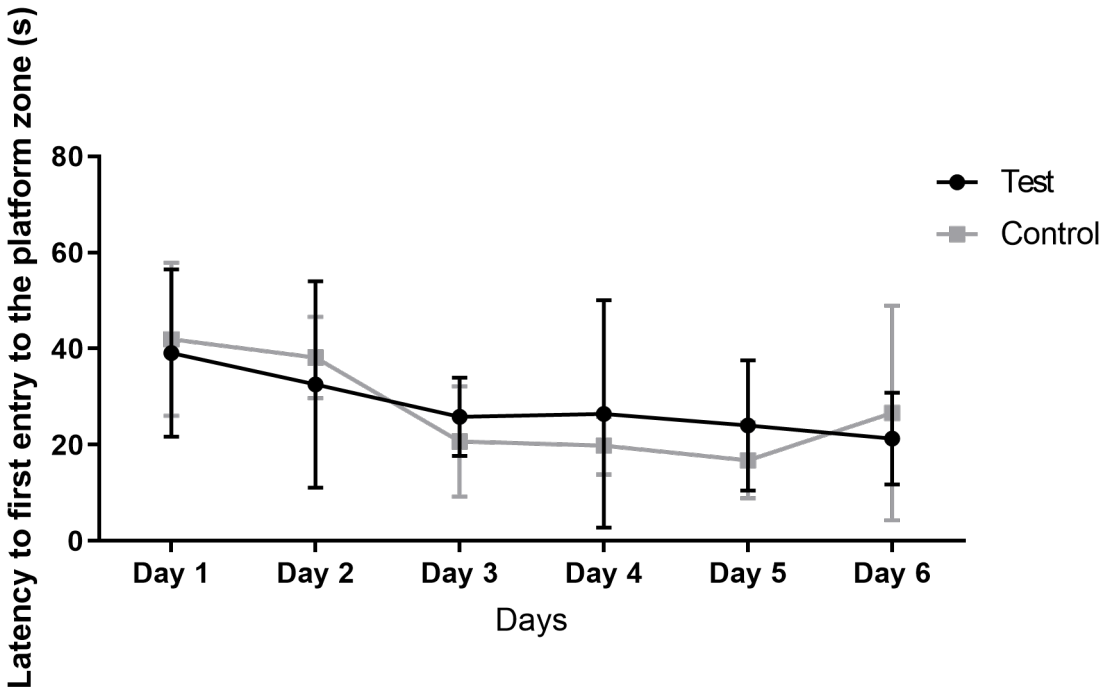

Figure 5.11. Latency times to the hidden platform in morris water maze experiments.

Similar to morris water maze experiment results, GPR139 ablation did not result in any significant differences between the test and control groups in per cent of time spent in open arms ($p = 0.5151$) and per cent of time spent in the closed arms ($p = 0.7697$) (Figure 5.12).

5.5.4. Open Field Test

Open field test measures general mobility, anxiety and exploration habits in rodents. If the mice are more anxious or their exploration habits are negatively affected due to treatment, they will spend less time in the center zone and travel distance will be lower. Similar to MWM and EPM tests, there are no significant differences between the test and control groups in distance traveled ($p = 0.6976$), number of entries to the center zone ($p = 0.08391$), average duration of visit to the center zone ($p = 0.2395$) and time spent in the center zone ($p = 0.2842$) measures (Figure 5.13).

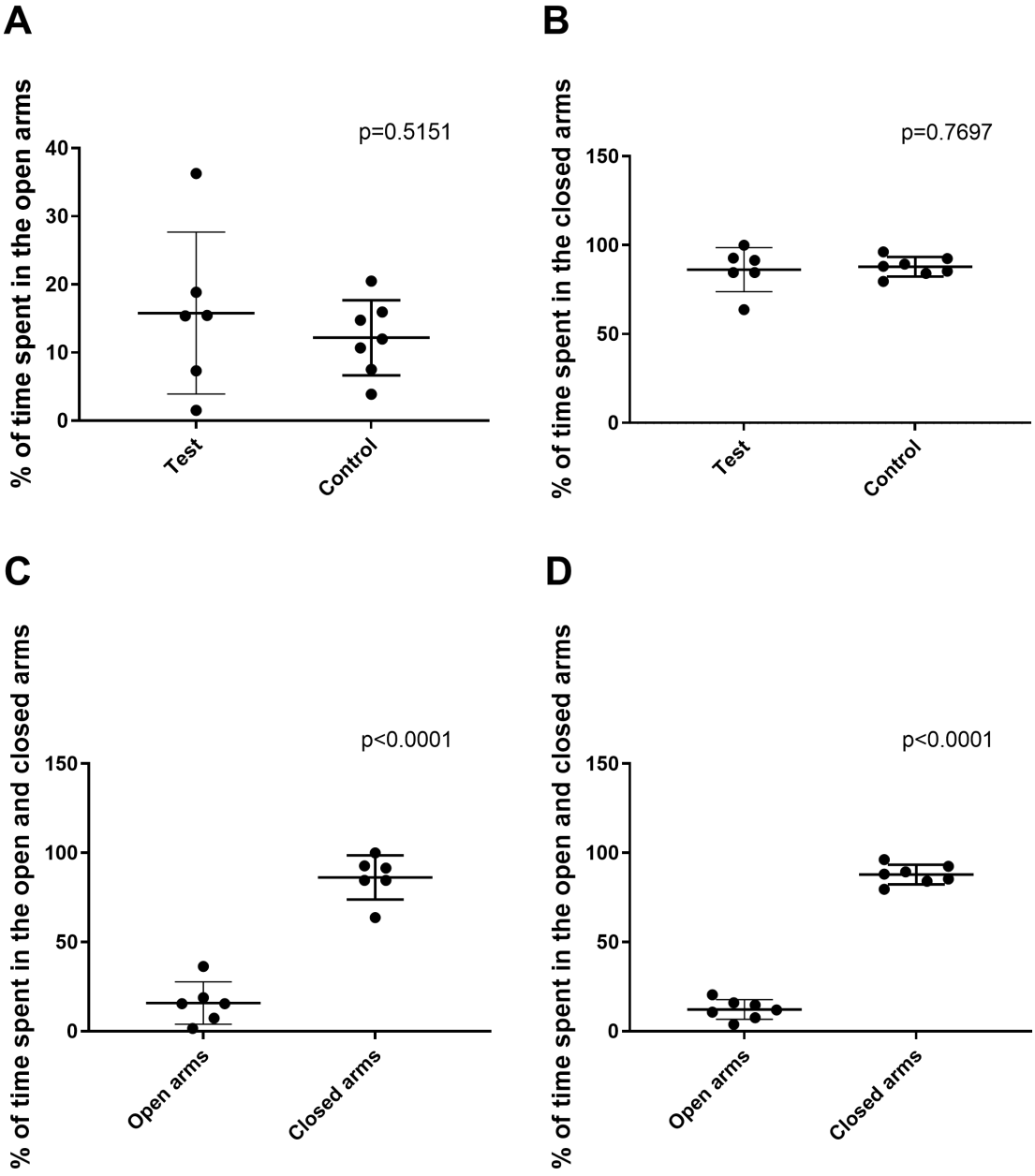

Figure 5.12. Percentage of time spent on open arms (a), closed arms (b), and comparison of percentage of time spent on either arms for the test (c) and control (d) groups observed in elevated plus maze experiments.

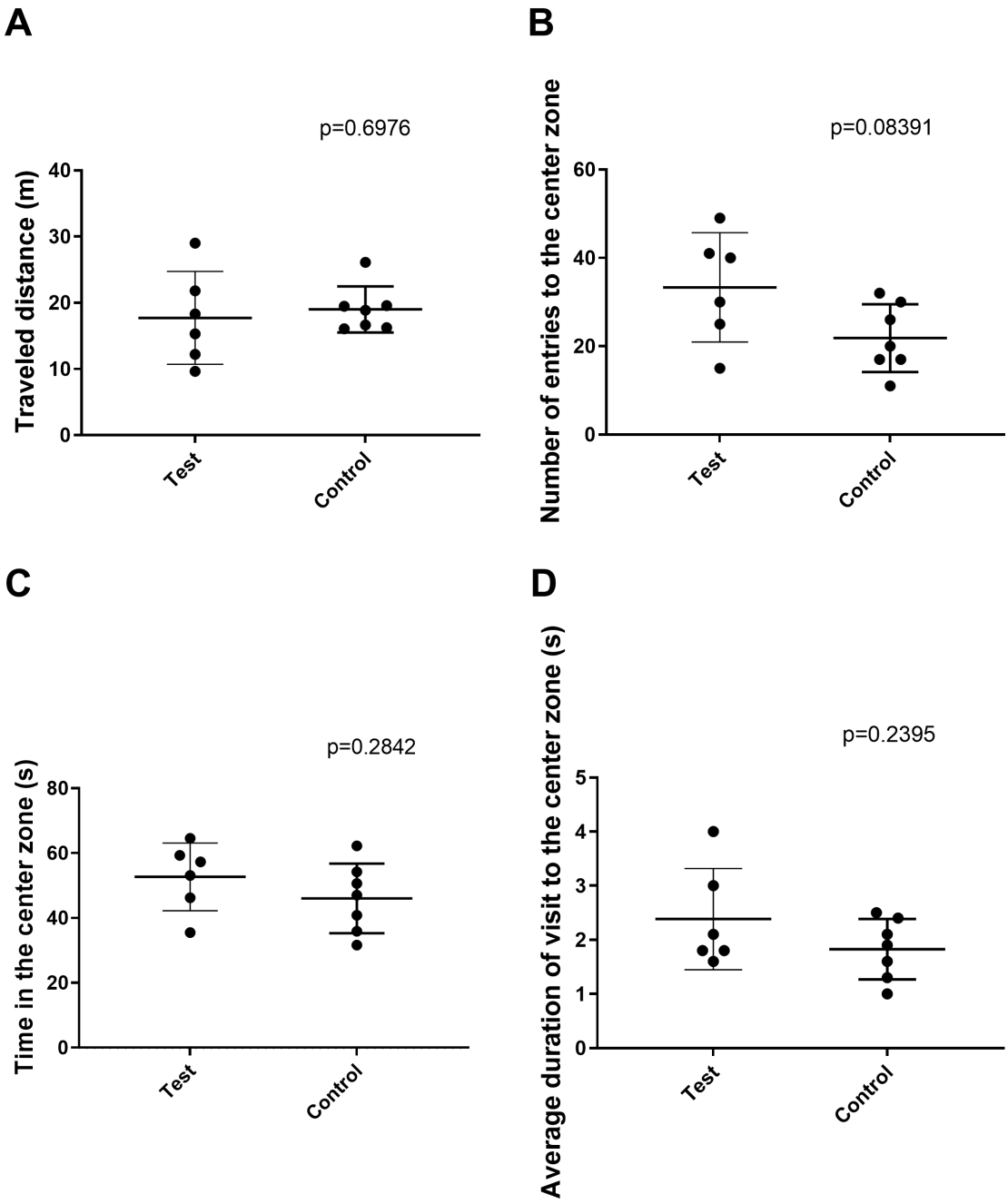

Figure 5.13. Traveled distance (a), number of entries to the center zone (b), time spent in the center zone (c) and average duration of visit to the center zone (d) obtained in the open field experiments.

5.5.5. Novel Object Recognition Test

Novel object recognition test measures recognition memory. After acclimation, mice are expected to get familiar with the fixed object. After introducing the novel object to the test chamber, they will prefer to explore the novel object rather than the already familiar fixed object. As can be seen in Figure 5.14, this expected behavior is observed both in test and control groups. Both groups spent similar amount of time on the fixed and novel objects, while the time spent on the novel object is higher. Anxious animals may refrain from exploration and spend less time on either object in this test but both groups spent similar amount of time on object exploration as can be seen in Figure 5.14c. Similar to other behavioral experiments, there are no significant differences between the test and control groups in time of interaction with the fixed object ($p = 0.3665$), the novel object ($p = 0.8194$) or either object ($p = 6325$). There were no significant differences in the calculated discrimination ratios ($p = 0.8746$).

5.5.6. Verification of Ablation

Western blot analysis was used to quantify the vinculin, Cas9, GFP and Gpr139 levels in test and control groups (Figure 5.15). Obtained images were quantified using ImageJ by normalizing the band intensities to vinculin (Figure 5.16). Both the blot images and quantification results showed similar levels of Cas9 and GFP proteins. Rosa26-floxed STOP-Cas9 knock-in mice show a Cre dependent expression of bicistronic Cas9 and GFP expression. Although the control group included in the study are injected with AAV containing Cre recombinase sequence, the injection protocol of two test group animals were unsuccessful and they show little to no Cas9 and GFP expression (Figure 5.15). These two animals were excluded from the quantification and behavioral experiment analyses.

Quantification of the blots show no significant differences for the Cas9 ($p = 0.2140$) and GFP ($p = 0.9315$) expression between the test and control groups. Gpr139 expression, on the other hand is significantly lower in the test group compared to the controls ($p = 0.0008$) indicating a successful ablation.

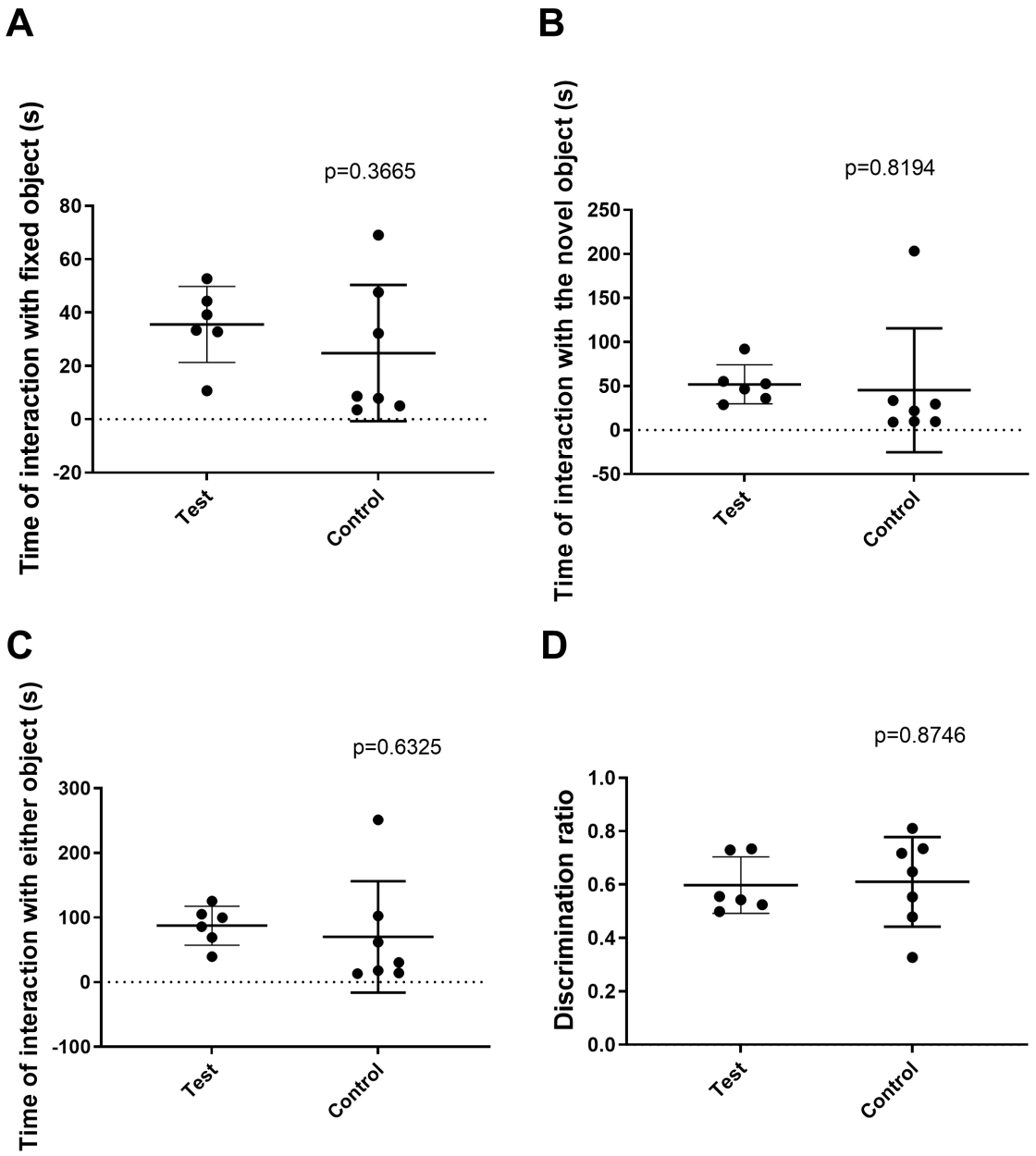

Figure 5.14. Time of interaction with the fixed object (a), novel object (b), either object (c), and discrimination ratio (d) observed in novel object recognition experiments.

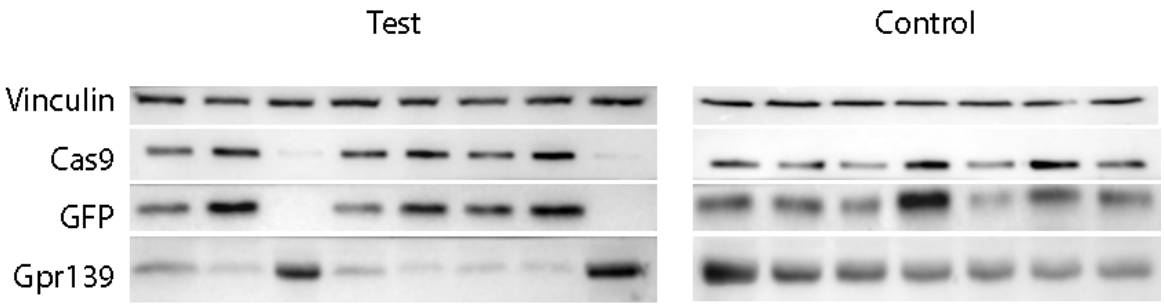

Figure 5.15. Western blot results for test and control groups. Vinculin (124 kDa) is used as loading control. GFP (27 kDa) and Cas9 (160 kDa) expression is Cre dependent and induced by the AAV in transgenic mice used in the study.

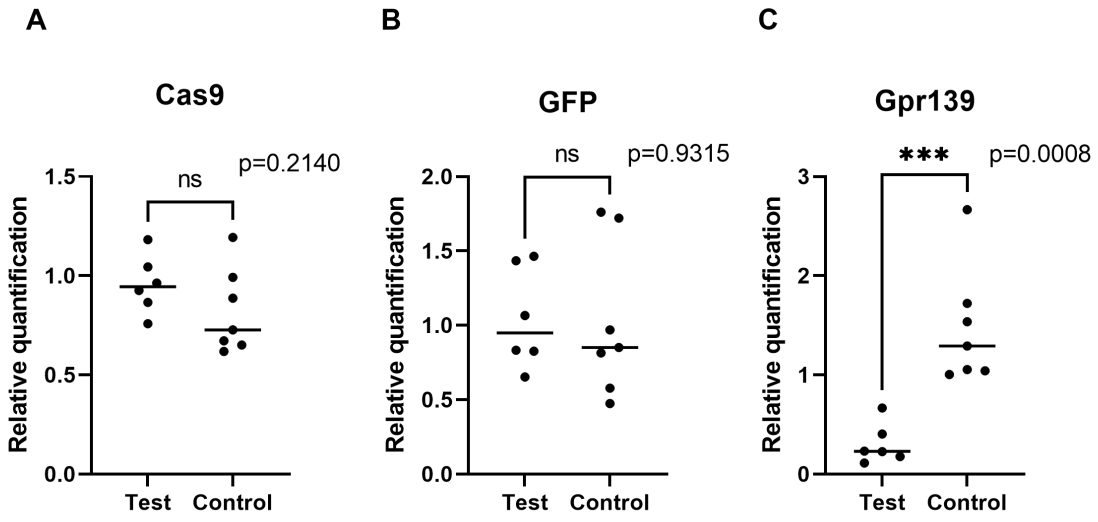

Figure 5.16. Quantification of western blot band intensities for Cas9 (a), GFP (b), and Gpr139 (c).

6. DISCUSSION

G protein coupled receptors are major drug targets in the pharmaceutical industry with more than 34% of currently marketed drugs targeting non-olfactory GPCRs [8]. More than 140 GPCRs are still categorized as orphans since their endogenous ligands are not yet identified [9]. Orphan GPCRs are an active field of research both from scientific and pharmaceutical standpoints. Scientific communities are interested in oGPCRs since they pose great opportunities in understanding areas in human physiology not yet determined. Pharmaceutical industry is actively researching the function of oGPCRs as well as their agonists and antagonists since they pose great financial opportunities in case the oGPCR in question is shown to be involved in the etiology of a disorder that is still untreatable with medication.

GPR139 was first reported as a local duplicate of GPR142 in 2003 [1], and reported as a separate receptor in 2005 [3, 5, 18]. At the time of its discovery, very little was known about GPR139: its homology with other rhodopsin family GPCRs is only 20-25% and it is mainly expressed in distinct areas of the central nervous system [18]. The same publication also showed that the receptor has differential expression in the mouse embryo brain in different developmental stages [18]. The latter finding together with the fact that the receptor's expression is limited to the central nervous system raised the possibility that GPR139 may play a role in brain development and/or function.

GPR139 still remains as an orphan GPCR. As expected, brain extracts have been shown to activate the receptor [18], its cognate ligand is still unknown. At the time of the start of our studies on GPR139, there were 18 publications reporting various aspects of the receptor. These publications include the original discovery articles [1,3,5,18,49], surrogate agonist and/or antagonist reports [10,19,20,23–26,50–52], and only 3 articles reporting GPR139's possible involvement in reduced locomotor activity [20], attention deficit hyperactivity disorder [21], and inattention [22].

Our initial interest in GPR139 was to identify its role in brain development. The possible role of GPR139 in brain development and/or function has been supported by several publications at the date of our initial study [20–22]. For that purpose we devised several lines of experiments including bioinformatic analyses of readily available datasets in the ENCODE database [53] in terms of the expression profile, DNA methylation and histone modifications, generation of a knock out mice model to investigate the function of GPR139 in mouse brain development, and *in vivo* ablation of GPR139 to investigate the effects of the receptor in adult mice.

Analysis of the transcript levels of *Gpr139* confirmed previous publications on the expression profile of the receptor in various tissues. *Gpr139* expression was indeed confined to the central nervous system (Figure 5.2 and there were significant differences between the transcript counts between different embryonic days (Table 5.1 indicating a possible role of GPR139 in brain development. During mammalian embryogenesis, expression profile of genes in tissues shapes the development of organs [54]. This data combined with the publications available at the time strengthened our hypothesis that GPR139 plays a role in brain development.

As the next step, we focused on how the expression of *Gpr139* is mediated in the developing mouse brain. For this purpose, we first employed the whole genome bisulfite sequencing data available on ENCODE. DNA methylation is a dynamic process and is one of the mechanisms that control gene expression by inhibiting the binding of transcription factors or recruiting them to prevent or allow the gene expression [55]. We analyzed the available dataset (Table 4.10) to obtain the methylation profile of the gene region including the regulatory region and predicted promoter region. The methylation profile did not show any significant differences between the time points in which the transcript levels are significantly different in the three brain sections included in the analysis (Figure 5.3). The same analysis showed changes in DNA methylation levels in the liver tissue, in which *Gpr139* is known not to be expressed. Taken together, these results suggest that the expression of *Gpr139* is not regulated, at least mainly, by DNA methylation.

It is not yet known if the high levels of methylation in the predicted promoter region of *Gpr139* has an inhibitory or promote the recruitment of proteins involved in its expression. Taken together with the active transcription and high transcript levels of the gene in the brain tissue, we speculate that the active methylation of the promoter region has the latter effect. In our effort to determine the mechanism(s) controlling the expression of *Gpr139*, we also analyzed the ChIP-Seq data available on the ENCODE database. Our analysis showed changing levels and a possible synergy between H3K4me3, H3K4me1, H3K9me3, H3K36me3, H3K27me3, H3K4me2, H3K9ac and H3K27ac modifications (Figure 5.4). Acetylation of H3K9 has been associated with active transcription by mediating a switch from transcription to elongation [56]. H3K4me3 is associated with transcriptional start sites of active genes [57]. H3K27 trimethylation and acetylation are markers of inactive and active transcription, respectively [57]. H3K4me3 and H3K27me3 play an important role in development and embryonic stem cell differentiation by acting against each other and creating bivalent chromatin [58]. Their antagonistic effects on gene activation allows the gene to be silenced (by H3K27me3) but not permanently (by H3K4me3). This bivalent nature allows genes to be "poised" against transcription and upon replacement of trimethylation with acetylation on H3K27, the gene becomes activated. This poised state is said to be important for embryonic stem cells in maintaining pluripotency, as well as for transcriptional regulation of genes that have important functions in development [58]. In hind-, mid- and fore-brain sections of the mouse brain, this phenomenon is clearly seen (Figure 5.4). H3K4me3 is observed throughout the developmental stages, indicating an "on" state of *Gpr139*, which is encountered by trimethylation of H3K27 in early stages. This H3K27me3 modification is then replaced by acetylation, upon which, transcript levels increase (Figure 5.4). This bivalent state is absent in liver tissue and only H3K27me3 modification is present throughout developmental stages, which indicate a permanent silencing of *Gpr139*.

Bioinformatic analyses we have performed strongly suggest that *Gpr139* is differentially expressed in developing mouse brain, has a wide expression profile in the central nervous system, and its expression is mainly controlled by histone modifications.

In order to examine the effects of GPR139 in brain development, we have devised a mouse knock-out experiment. In this line of experiments, the aim was to create a *Gpr139* knock-out mouse model followed by morphological examinations and behavioral test to measure the possible effects. Due to lack of information in the literature and an already available knock out animal model at the time of initiation of our study, we anticipated two possible outcomes of *Gpr139* knock out in terms of development: (A) the effect could be detrimental to the embryo and result in embryonic death or a similar effect that will prevent obtaining live pups, or (B) there will be tolerable or no effect on the embryonic development which will allow us to obtain live *Gpr139* knock out animals. We have devised possible courses of action for both scenarios. In case the treatment resulted in embryonic death, the day at which the embryonic death occurred would be investigated, and if the death occurred at a stage at which the embryo and its brain is developed large enough to be subjected to morphological analyses as well as investigation by various molecular biology techniques, we would try to examine why and how the embryonic death occurred. If the treatment did not result in embryonic death and we could obtain live pups, same molecular techniques as well as behavioral experiments outlined above would be employed.

We chose to employ CRISPR-Cas9 technology for creation of the knock-out mouse model for its efficiency, ease of application and robustness [42]. Customization of Cas9 compared to conventional methods such as TALEN is much simpler and faster as it only involves determining the suitable targeting sites, designing the guide sequence, cloning the guide sequence into a suitable Cas9 vector and performing *in vitro* transcription while conventional methods much more hands on time and doesn't offer same level of customizability [42]. The actual "knocking out" procedure of Cas9 also involves fewer steps during embryo manipulation and animal breeding. With Cas9 method, fertilized embryos are isolated, Cas9 mRNA and sgRNA are injected into the cytoplasm, embryos are cultivated *in vitro* until they reach 8 cell or blastocyst stage, and transferred to surrogate mothers.

In the conventional methodology, as opposed to CRISPR-Cas9 technology, main steps are isolating embryonic stem cells from the blastocyst, cultivating them *in vitro*, introducing the sequence that will replace the wild type sequence via electroporation or microinjection, selecting the cells with the new sequence using the introduced selection marker, transferring the selected cells into the blastocyst and transferring the chimeric blastocysts into the pseudo-pregnant surrogate females. Cas9 method also does not require crossing chimeric mice with wild type mice to obtain heterozygous mutants and another cross breeding that will yield homozygous mutants since it results in homozygous mutants immediately in the first generation [42].

We have evaluated the efficiency of deletion at the targeted site on *Gpr139* by our Cas9/sgRNA construct, we have flash frozen single blastocysts from the test and control groups, amplified the targeted region by PCR and subjected the amplicons to SURVEYOR assay and sequencing. Our results showed 100% success rate in deletion (Figures 5.6 and 5.7) and no visible abnormalities in the embryo. When the injected embryos were transferred to the surrogate mothers, however, we weren't able to obtain live pups which may stem from (A) embryonic death or (B) failing to successfully transfer the embryos into the uteri. First week after the transfer, however, one of the surrogate mothers gained 2.4 g and built a nest. This increase in weight and nesting behavior could be the result of induced pseudo pregnancy or successful embryo transfer. To further analyze the underlying reason, we sacrificed the mouse and performed necropsy. Upon detailed analysis of the reproductive system, we did not see obvious signs of embryo attachment and growth. We speculated that the transferred embryos did not attach to the uterus or did not properly develop but we did not have enough data to reach a conclusion. Control embryos transferred to the surrogate mother, on the other hand, resulted in live pups (Figure 5.8).

Although we have achieved significant progress in generation of knock-out mouse model, this branch of the project was discontinued due to technical difficulties, budgetary issues and a recent publication [59] that created the knock-out model using a similar approach and performed the behavioral tests that we were planning in a larger context.

According to this publication, *Gpr139* knock-out mice do not show any observable differences in terms of growth, brain morphology and various behavioral aspects. According to this publication, *Gpr139* knock-out mice do not show any observable differences in terms of growth, brain morphology, body composition in terms of weight, fat and muscle, as well as behavioral aspects such as locomotor activity, habituation, motor coordination/learning [59]. The impact of this publication, however, goes beyond showing that the *Gpr139* does not have any observable effects in mouse development or various measures of behavior such as learning and anxiety. Authors have shown GPR139 receptor is coexpressed with μ-opioid receptor (MOR), forms dimers with MOR that inhibits G protein signaling which taken together results in a modulatory effect on response to opioids [59]. They, perhaps more importantly, have also shown that activation of GPR139 by the small molecule agonist JNJ-63533054 resulted in suppression of morphine self-administration in wild type mice [59]. This publication is one of the first articles that showed the importance of GPR139 and its potential use in the pharmacological industry both in treatments involving opioids and reducing effects of withdrawal in opioid addiction.

Although the knock out model created by Dandan et al. (2019) [59] does not show any observable effect on brain development, nociception, learning, locomotor activity and habituation, this lack of effect might be due to the relatively new concept of gene compensation. Different than dosage compensation, gene compensation can be defined as the functions of a gene are taken over, or compensated, by other gene or genes in the case of deleterious mutations that result in nonfunctional or malfunctioning gene products [60, 61]. Well established phenotypes observed in morphants have been reported to be unobserved in mutant animal models [60–62]. General logic dictates a knock-out organism should present a more severe phenotype compared to a knock-down, or morphant, organism since the gene responsible for the phenotype is non-functional or missing completely rather than having a reduced product levels. The opposite of this expected outcome is sometimes, but not always, observed in animal models [63]. We speculated that gene compensation could be the reason for not observing any phenotypical differences in the aspects stated earlier reported by Dandan et al. (2019) [59].

If this was the case, ablation of *Gpr139* in adult mice experiments could possibly yield different results reported by Dandan et al. (2019) [59]. Even though the ablation procedure used in our study employs Cas9 technology and manipulates the genome rather than modulating the gene expression in other methods such as morpholinos, RNAi, or tetracycline induced repression, due to the imperfect silencing which results in 10-to-20% gene expression and relatively short time frames between ablation and experiments compared to knock out models, this line of experiments could potentially yield different results.

Ablation of *Gpr139* yielded around 80% reduction of protein levels (Figures 5.15 and 5.16) which is in line with previously reported ablation procedures using similar methodologies [64]. Although the ablation was successful, we did not observe any significant differences between the test group and the control animals in morris water maze experiments (Figure 4.21), elevated plus maze experiments (Figure 5.12), novel object recognition experiments (Figure 5.14), or open field experiments (Figure 5.13).

Morris water maze test measures the animals' spatial learning capabilities. Rodents inherently prefer standing on solid ground compared to swimming and morris water maze is designed to encourage this instinct further by reducing the water temperature to levels that causes discomfort. Animals are dropped into the water tank in a non-repeating pattern (Table 4.21) in successive days to prevent learning by repetition and allowing learning by visual cues present in the experiment room. Animals are expected to spend less time in consecutive days since they are expected to learn the spatial position of the hidden platform using aforementioned visual cues. In our experiments, we did not observe differences between the test and control groups ($p = 0.8415$). The high p value between the test and control groups suggests that ablation of GPR139 does not affect spatial learning, memory, or any measures that can directly or indirectly affect the performance of mice in morris water maze (Figure 5.11).

Similar to morris water maze, elevated plus maze (Figure 5.12) (time spent in open arms: $p = 0.5151$, time spent in closed arms: $p = 0.7697$) and open field tests (Figure 5.13) (distance traveled: $p = 0.6976$, number of entries to the center zone: $p = 0.08391$, average duration of visit to the center zone: $p = 0.2395$, time spent in the center zone: $p = 0.2842$) did not yield any significant differences between test and control groups in terms of anxiety. Mice are curious but cautious by nature. When introduced to a non-familiar environment, they will explore the new area while avoiding potential threats such as open spaces and heights. Open field test measures anxiety by comparing the time spent near the center field of the test chamber which is "danger prone" since the animals are exposed and the time spent near the sides and corners which are relatively "safer" since the animals are less exposed. Though not statistically significant, the most discernible difference between the test and control groups in the open field experiments is the number of entries to the center zone where the control group shows fewer number of entries (mean for control group: 21.86, mean for test group: 33.33, 95% CI: -24.88 to 1.928). The p value observed in this measure is much lower than those observed in other measures in the open field test and potentially could indicate that the test group animals are more curious rather than cautious compared to the test group. Time spent in the center zone and and the average duration of visits to the center zone measures, however, have higher p values indicating similar behavioral patterns between the test and control groups. Since the time spent in the center zone is not statistically different between the two groups, our conclusion for the animals' preference between curiosity vs cautiousness is not different between the test and control groups. The distance travelled also used as a measure for anxiety since anxious animals prefer to stay in a safer place rather than exploring, in which the difference observed between the two groups is not statistically different suggesting that the ablation of GPR139 did not have significant differences in this measure. Elevated plus maze uses open and closed arms as well as elevation to measure the anxiety. Similar to open field test, animals are expected to explore both the open and closed arms even though the open arms pose as a potential stress factor for the animal by both being an open space without a shelter from threats and visibly elevated from the ground.

For both experiment groups, as expected, the closed arms are significantly preferred over open arms (Figure 5.12c and d) and there were no significant differences between the time spent in the open or closed arms between the two groups (Figure 5.12a and b). Novel object recognition test measures animal's recognition memory. Thanks to their curious nature, mice will spend more time in exploring novel objects rather than known objects. This test measures the recognition memory by first introducing the mice to the previously acclimated test chamber which contains two identical objects, and in consecutive trials changing one of the objects with an unfamiliar one. Mice are expected to spend more time on the novel object. The discrimination ratio obtained in our experiments shows that this expected behavior is observed both in the test and control groups with no significant differences ($p = 0.8746$, Figure 5.14d). The discrimination ratio, however, does not take the total time spent in interacting with either object and only the ratios of the difference between total time spent on the novel object and the fixed object to total time spent in either object. The time of interaction with the fixed (Figure 5.14a, $p = 0.3665$) and novel objects (Figure 5.14b, $p = 0.8194$), and the total time spent on interacting with either object (Figure 5.14c, $p = 0.6325$) clearly shows there are no significant differences in preference of the animals in either group in terms of time spent in object interaction. Taken together, these results indicate that the ablation of GPR139 does not affect the recognition memory in mice.

Behavioral experiments showed no differences between the test and control groups. These results are in line with previous report by Dandan et al. (2019) [59]. As discussed above, that publication involved knock out mice and contained more behavioral experiments none of which resulted in a significant difference between the knock out and wild type animals [59]. Since the *in vivo* ablation of *Gpr139* in adult mice performed by us and *Gpr139* knock out resulted in similar outcomes in terms of the behavioral measures examined in this study, gene compensation is unlikely to be involved in reported phenotypes and GPR139 is actually not involved in recognition memory, spatial learning, attention and anxiety. Gene compensation usually involves homologous genes or genes with similar biochemical functions [62].

Gpr139 is known to have very low homology with other members of the rhodopsin family GPCRs and only about 50% homology with *Gpr142* [18]. Our results combined with the similar results of the knock out study as well as lack of a homologous gene, we think the gene compensation is not involved in published phenotypes and GPR139 is in fact not involved in behavioral aspects reported by Dandan et al. (2019) [59] and this study.

At the time of planning and initiation of this study, the literature on GPR139 and its function(s) were limited and its possible role in brain development, learning, anxiety and memory haven't been investigated. This study was aimed to shed light on these missing pieces surrounding GPR139, an under-investigated and relatively newly identified orphan receptor. During the course of this study, however, we have encountered various setbacks which created weaknesses. First setback was encountered during the generation of the knock out mouse model. Knock out mouse generation was performed in collaboration with Istanbul University Faculty of Veterinary Sciences Department of Reproduction and Artificial Insemination (IU RAI). Although this collaboration was done in good faith and our collaborators showed utmost interest in our work and provided us with their technical facilities and knowledge without reservations, their busy schedule and the distance between the two facilities has created difficulties in scheduling experiments, which in turn caused the experiments to be performed in longer intervals than ideal. More over, the budgetary constraints and increases in the costs of consumables limited access to reagents and eventually the number of trials. In addition, COVID 19 pandemic caused the largest set back due to limitations in travel and co-habitation of workspaces. Combined with publications performing the same set of experiments in a larger settings, knock out experiments were cancelled without reaching conclusive results. The bioinformatic analyses and *in vivo* ablation experiments, on the other hand, were completed without major issues and provided useful data. RNAseq analyses provided information on the expression pattern of *Gpr139* in the developing mouse brain and showed a clear differential expression pattern.

DNA methylation and histone modification analyses showed that this differential expression was governed by histone modification and not by DNA methylation. During the *In vivo* ablation experiments, as in knock out experiments, we have encountered budgetary limitations due to increased cost of reagents and the FloxP-Cas9 mice, as well as the COVID 19 restrictions, the number of animals that could be used in the study was lower than initially planned reducing the statistical power of this line of experiments.

7. CONCLUSION

In conclusion, results of this study clearly showed that *Gpr139* has differential expression in the developing mouse and its expression is restricted to the central nervous system, its expression is most likely regulated by histone modifications, and ablation of *Gpr139* has no discernible effect on spatial learning, locomotor activity, recognition memory and anxiety. Considering the recent developments and interests in the literature, discovering the pharmaceutical importance of GPR139 rather than discovering endogenous ligand(s) of GPR139 and its native function will have more translational value. In the coming years, we expect GPR139 to be a viable target for small molecule drugs for treatment of opioid addiction, schizophrenia, ADHD, and possibly Parkinson's disease. Although there are multiple investigations on GPR139 in these diseases and conditions, there may still be yet-to-be explored functions and involvements of GPR139 which may provide invaluable insight into various diseases and potentially clear the way for their treatment.

REFERENCES

1. Fredriksson, R., M. C. Lagerström, L.-G. Lundin and H. B. Schiöth, "The G-Protein-Coupled Receptors in the Human Genome Form Five Main Families. Phylogenetic Analysis, Paralogon Groups, and Fingerprints", *Molecular Pharmacology*, Vol. 63, No. 6, pp. 1256–1272, 2003.

2. Civelli, O., Y. Saito, Z. Wang, H.-P. Nothacker and R. K. Reinscheid, "Orphan GPCRs and Their Ligands", *Pharmacology & Therapeutics*, Vol. 110, No. 3, pp. 525–532, 2006.

3. Gloriam, D. E. I., H. B. Schiöth and R. Fredriksson, "Nine New Human Rhodopsin Family G-Protein Coupled Receptors: Identification, Sequence Characterisation And Evolutionary Relationship", *Biochimica et Biophysica Acta - General Subjects*, Vol. 1722, No. 3, pp. 235–246, 2005.

4. Palczewski, K., T. Kumasaka, T. Hori, C. A. Behnke, H. Motoshima, B. A. Fox, I. Le Trong, D. C. Teller, T. Okada, R. E. Stenkamp, M. Yamamoto and M. Miyano, "Crystal Structure of Rhodopsin: A G Protein-Coupled Receptor.", *Science (New York, N.Y.)*, Vol. 289, No. 5480, pp. 739–745, 2000.

5. Matsuo, A., S. I. Matsumoto, M. Nagano, K. H. Masumoto, J. Takasaki, M. Matsumoto, M. Kobori, M. Katoh and Y. Shigeyoshi, "Molecular Cloning and Characterization of a Novel Gq-Coupled Orphan Receptor GPRg1 Exclusively Expressed in the Central Nervous System", *Biochemical and Biophysical Research Communications*, Vol. 331, No. 1, pp. 363–369, 2005.

6. Mombaerts, P., "Genes and Ligands for Odorant, Vomeronasal and Taste Receptors.", *Nature Reviews. Neuroscience*, Vol. 5, No. 4, pp. 263–278, 2004.

7. Huang, Y., N. Todd and A. Thathiah, "The Role of GPCRs in Neurodegenerative Diseases: Avenues for Therapeutic Intervention.", *Current Opinion in Pharmacol-*

ogy, Vol. 32, pp. 96–110, 2017.

8. Hauser, A. S., M. M. Attwood, M. Rask-Andersen, H. B. Schiöth and D. E. Gloriam, "Trends in GPCR Drug Discovery: New Agents, Targets and Indications.", *Nature Reviews. Drug Discovery*, Vol. 16, No. 12, pp. 829–842, 2017.

9. Azam, S., M. E. Haque, M. Jakaria, S.-H. Jo, I.-S. Kim and D.-K. Choi, "G-Protein-Coupled Receptors in CNS: A Potential Therapeutic Target for Intervention in Neurodegenerative Disorders and Associated Cognitive Deficits.", *Cells*, Vol. 9, No. 2, 2020.

10. Isberg, V., K. B. Andersen, C. Bisig, G. P. H. Dietz, H. Bruner-Osborne and D. E. Gloriam, "Computer-Aided Discovery of Aromatic L-Alpha-Amino Acids as Agonists of the Orphan G Protein-Coupled Receptor GPR139", *Journal of Chemical Information and Modeling*, Vol. 54, No. 6, pp. 1553–1557, 2014.

11. Stiles, J. and T. L. Jernigan, "The Basics of Brain Development.", *Neuropsychology Review*, Vol. 20, No. 4, pp. 327–348, 2010.

12. Baer, A. S., Y. A. Syed, S. U. Kang, D. Mitteregger, R. Vig, C. ffrench Constant, R. J. M. Franklin, F. Altmann, G. Lubec and M. R. Kotter, "Myelin-Mediated Inhibition of Oligodendrocyte Precursor Differentiation Can be Overcome by Pharmacological Modulation of Fyn-RhoA and Protein Kinase C Signalling", *Brain*, Vol. 132, No. 2, pp. 465–481, 2009.

13. Kakegawa, W., N. Mitakidis, E. Miura, M. Abe, K. Matsuda, Y. H. Takeo, K. Kohda, J. Motohashi, A. Takahashi, S. Nagao, S.-i. Muramatsu, M. Watanabe, K. Sakimura, A. R. Aricescu and M. Yuzaki, "Anterograde C1ql1 Signaling is Required in Order to Determine and Maintain a Single-Winner Climbing Fiber in the Mouse Cerebellum.", *Neuron*, Vol. 85, No. 2, pp. 316–329, 2015.

14. Lanoue, V., A. Usardi, S. M. Sigoillot, M. Talleur, K. Iyer, J. Mariani, P. Isope, G. Vodjdani, N. Heintz and F. Selimi, "The Adhesion-GPCR BAI3, a Gene Linked

to Psychiatric Disorders, Regulates Dendrite Morphogenesis In Neurons", *Molecular Psychiatry*, Vol. 18, No. 8, pp. 943–950, 2013.

15. Chai, G., A. M. Goffinet and F. Tissir, "Celsr3 and Fzd3 in Axon Guidance", *The International Journal of Biochemistry & Cell Biology*, Vol. 64, pp. 11–14, 2015.

16. Ackerman, S. D., C. Garcia, X. Piao, D. H. Gutmann and K. R. Monk, "The Adhesion GPCR Gpr56 Regulates Oligodendrocyte Development Via Interactions with Gα12/13 and RhoA", *Nature Communications*, Vol. 6, No. 1, p. 6122, 2015.

17. Ehrlich, A. T., G. Maroteaux, A. Robe, L. Venteo, M. T. Nasseef, L. C. van Kempen, N. Mechawar, G. Turecki, E. Darcq and B. L. Kieffer, "Expression Map of 78 Brain-Expressed Mouse Orphan GPCRs Provides a Translational Resource for Neuropsychiatric Research", *Communications Biology*, Vol. 1, No. 1, p. 102, 2018.

18. Süsens, U., I. Hermans-Borgmeyer, J. Urny and H. C. Schaller, "Characterisation and Differential Expression of Two Very Closely Related G-Protein-Coupled Receptors, GPR139 and GPR142, in Mouse Tissue and During Mouse Development", *Neuropharmacology*, Vol. 50, No. 4, pp. 512–520, 2006.

19. Andersen, K. B., J. Leander Johansen, M. Hentzer, G. P. Smith and G. P. H. Dietz, "Protection of Primary Dopaminergic Midbrain Neurons by GPR139 Agonists Supports Different Mechanisms of MPP+ and Rotenone Toxicity", *Frontiers in Cellular Neuroscience*, Vol. 10, p. 164, 2016.

20. Liu, C., P. Bonaventure, G. Lee, D. Nepomuceno, C. Kuei, J. Wu, Q. Li, V. Joseph, S. W. Sutton, W. Eckert, X. Yao, L. Yieh, C. Dvorak, N. Carruthers, H. Coate, S. Yun, C. Dugovic, A. Harrington and T. W. Lovenberg, "GPR139, an Orphan Receptor Highly Enriched in the Habenula and Septum, Is Activated by the Essential Amino Acids Tryptophan and Phenylalanine", *Molecular Pharmacology*, Vol. 88, No. 5, pp. 911 LP – 925, 2015.

21. Castellani, C. a., Z. Awamleh, M. G. Melka, R. L. O'Reilly and S. M. Singh, "Copy Number Variation Distribution in Six Monozygotic Twin Pairs Discordant for Schizophrenia", *Twin Research and Human Genetics*, Vol. 17, No. 02, pp. 108–120, 2014.

22. Ebejer, J. L., D. L. Duffy, J. van der Werf, M. J. Wright, G. Montgomery, N. A. Gillespie, I. B. Hickie, N. G. Martin and S. E. Medland, "Genome-Wide Association Study of Inattention and Hyperactivity–Impulsivity Measured as Quantitative Traits", *Twin Research and Human Genetics*, Vol. 16, No. 02, pp. 560–574, 2013.

23. Wang, J., L.-y. Zhu, Q. Liu, M. Hentzer, G. P. Smith and M.-w. Wang, "High-Throughput Screening of Antagonists for the Orphan G-Protein Coupled Receptor GPR139", *Acta Pharmacologica Sinica*, Vol. 36, No. 2, pp. 1–5, 2015.

24. Dvorak, C. A., H. Coate, D. Nepomuceno, M. Wennerholm, C. Kuei, B. Lord, D. Woody, P. Bonaventure, C. Liu, T. Lovenberg and N. I. Carruthers, "Identification and SAR of Glycine Benzamides as Potent Agonists for the GPR139 Receptor", *ACS Medicinal Chemistry Letters*, Vol. 6, No. 9, pp. 1015–1018, 2015.

25. Hu, L. A., P. M. Tang, N. K. Eslahi, T. Zhou, J. Barbosa and Q. Liu, "Identification of Surrogate Agonists and Antagonists for Orphan G-Protein-Coupled Receptor GPR139.", *Journal of Biomolecular Screening*, Vol. 14, No. 7, pp. 789–797, 2009.

26. Shi, F., J. K. Shen, D. Chen, K. Fog, K. Thirstrup, M. Hentzer, J. J. Karlsson, V. Menon, K. A. Jones, K. E. Smith and G. Smith, "Discovery and SAR of a Series of Agonists at Orphan G Protein-Coupled Receptor 139", *ACS Medicinal Chemistry Letters*, Vol. 2, No. 4, pp. 303–306, 2011.

27. Dao, M., H. M. Stoveken, Y. Cao and K. A. Martemyanov, "The Role of Orphan Receptor GPR139 in Neuropsychiatric Behavior.", *Neuropsychopharmacology : Official Publication of the American College of Neuropsychopharmacology*, 2021.

28. Kuhne, S., A. Nøhr, A. Marek, T. Elbert, A. Klein, H. Bräuner-Osborne, P. Wellen-

dorph and D. Pedersen, "Radiosynthesis and Characterisation of a Potent and Selective GPR139 Agonist Radioligand", *RSC Adv.*, Vol. 6, 2015.

29. Hu, H., Y. Cui and Y. Yang, "Circuits and Functions of the Lateral Habenula in Health and in Disease", *Nature Reviews Neuroscience*, Vol. 21, No. 5, pp. 277–295, 2020.

30. Andres, K. H., M. V. Düring and R. W. Veh, "Subnuclear Organization of the Rat Habenular Complexes", *Journal of Comparative Neurology*, Vol. 407, No. 1, pp. 130–150, 1999.

31. Viswanath, H., A. Q. Carter, P. R. Baldwin, D. L. Molfese and R. Salas, "The Medial Habenula: Still Neglected", *Frontiers in Human Neuroscience*, Vol. 7, p. 931, 2014.

32. Otsu, Y., E. Darcq, K. Pietrajtis, F. Mátyás, E. Schwartz, T. Bessaih, S. Abi Gerges, C. V. Rousseau, T. Grand and S. Dieudonné, "Control of Aversion by Glycine-Gated GluN1/GluN3A NMDA Receptors in the Adult Medial Habenula", *Science*, Vol. 366, No. 6462, pp. 250–254, 2019.

33. Li, F. and J. Z. Tsien, "Memory and the NMDA Receptors", *The New England Journal of Medicine*, Vol. 361, No. 3, p. 302, 2009.

34. Bruinenberg, V., E. van der Goot, D. Vliet, M. Groot, P. Mazzola, M. Heiner Fokkema, M. Van Faassen, F. Spronsen and E. Van der Zee, "The Behavioral Consequence of Phenylketonuria in Mice Depends on the Genetic Background", *Front Behav Neurosci*, Vol. 10, p. 233, 2016.

35. Koch, R., R. Moats, F. Guttler, P. Guldberg and M. Nelson, "Blood-Brain Phenylalanine Relationships in Persons with Phenylketonuria.", *Pediatrics*, Vol. 106, No. 5, pp. 1093–6, 2000.

36. Murphy, A., "Croll-Kalish SKOR3 Like-Proteins and Methods of Modu-

lating KOR3L-Mediated Activity.", *Regeneron Pharmaceuticals Inc. Patent WO2004/074841 A2*, 2004.

37. Wang, D., H. M. Stoveken, S. Zucca, M. Dao, C. Orlandi, C. Song, I. Masuho, C. Johnston, K. J. Opperman, A. C. Giles, M. S. Gill, E. A. Lundquist, B. Grill and K. A. Martemyanov, "Genetic Behavioral Screen Identifies an Orphan Anti-Opioid System", *Science*, Vol. 365, No. 6459, pp. 1267–1273, 2019.

38. Stoveken, H. M., S. Zucca, I. Masuho, B. Grill and K. A. Martemyanov, "The Orphan Receptor Gpr139 Signals Via G(q/11) to Oppose Opioid Effects.", *The Journal of Biological Chemistry*, Vol. 295, No. 31, pp. 10822–10830, 2020.

39. Yin, W., D. Han, P. Khudyakov, R. Behrje, J. Posener, A. Laurenza and D. Arkilo, "A Phase 1 Study to Evaluate the Safety, Tolerability and Pharmacokinetics of TAK 041 in Healthy Participants and Patients with Stable Schizophrenia", *British Journal of Clinical Pharmacology*, 2022.

40. Dunham, I., A. Kundaje, S. F. Aldred, P. J. Collins, C. A. Davis, F. Doyle, C. B. Epstein, S. Frietze, J. Harrow, R. Kaul, J. Khatun, B. R. Lajoie, S. G. Landt, B.-K. Lee, F. Pauli, K. R. Rosenbloom, P. Sabo, A. Safi, A. Sanyal, N. Shoresh, J. M. Simon, L. Song, N. D. Trinklein, R. C. Altshuler, E. Birney, J. B. Brown, C. Cheng, S. Djebali, X. Dong, I. Dunham, J. Ernst, T. S. Furey, M. Gerstein, B. Giardine, M. Greven, R. C. Hardison, R. S. Harris, J. Herrero, M. M. Hoffman, S. Iyer, M. Kellis, J. Khatun, P. Kheradpour, A. Kundaje, T. Lassmann, Q. Li, X. Lin, G. K. Marinov, A. Merkel, A. Mortazavi, S. C. J. Parker, T. E. Reddy, J. Rozowsky, F. Schlesinger, R. E. Thurman, J. Wang, L. D. Ward, T. W. Whitfield, S. P. Wilder, W. Wu, H. S. Xi, K. Y. Yip, J. Zhuang, B. E. Bernstein, E. Birney, I. Dunham, E. D. Green, C. Gunter, M. Snyder, M. J. Pazin, R. F. Lowdon, L. A. L. Dillon, L. B. Adams, C. J. Kelly, J. Zhang, J. R. Wexler, E. D. Green, P. J. Good, E. A. Feingold, B. E. Bernstein, E. Birney, G. E. Crawford, J. Dekker, L. Elnitski, P. J. Farnham, M. Gerstein, M. C. Giddings, T. R. Gingeras, E. D. Green, R. Guigó, R. C. Hardison, T. J. Hubbard, M. Kellis, W. J. Kent, J. D.

Lieb, E. H. Margulies, R. M. Myers, M. Snyder, J. A. Stamatoyannopoulos, S. A. Tenenbaum, Z. Weng, K. P. White, B. Wold, J. Khatun, Y. Yu, J. Wrobel, B. A. Risk, H. P. Gunawardena, H. C. Kuiper, C. W. Maier, L. Xie, X. Chen, M. C. Giddings, B. E. Bernstein, C. B. Epstein, N. Shoresh, J. Ernst, P. Kheradpour, T. S. Mikkelsen, S. Gillespie, A. Goren, O. Ram, X. Zhang, L. Wang, R. Issner, M. J. Coyne, T. Durham, M. Ku, T. Truong, L. D. Ward, R. C. Altshuler, M. L. Eaton, M. Kellis, S. Djebali, C. A. Davis, A. Merkel, A. Dobin, T. Lassmann, A. Mortazavi, A. Tanzer, J. Lagarde, W. Lin, F. Schlesinger, C. Xue, G. K. Marinov, J. Khatun, B. A. Williams, C. Zaleski, J. Rozowsky, M. Röder, F. Kokocinski, R. F. Abdelhamid, T. Alioto, I. Antoshechkin, M. T. Baer, P. Batut, I. Bell, K. Bell, S. Chakrabortty, X. Chen, J. Chrast, J. Curado, T. Derrien, J. Drenkow, E. Dumais, J. Dumais, R. Duttagupta, M. Fastuca, K. Fejes-Toth, P. Ferreira, S. Foissac, M. J. Fullwood, H. Gao, D. Gonzalez, A. Gordon, H. P. Gunawardena, C. Howald, S. Jha, R. Johnson, P. Kapranov, B. King, C. Kingswood, G. Li, O. J. Luo, E. Park, J. B. Preall, K. Presaud, P. Ribeca, B. A. Risk, D. Robyr, X. Ruan, M. Sammeth, K. S. Sandhu, L. Schaeffer, L.-H. See, A. Shahab, J. Skancke, A. M. Suzuki, H. Takahashi, H. Tilgner, D. Trout, N. Walters, H. Wang, J. Wrobel, Y. Yu, Y. Hayashizaki, J. Harrow, M. Gerstein, T. J. Hubbard, A. Reymond, S. E. Antonarakis, G. J. Hannon, M. C. Giddings, Y. Ruan, B. Wold, P. Carninci, R. Guigó, T. R. Gingeras, K. R. Rosenbloom, C. A. Sloan, K. Learned, V. S. Malladi, M. C. Wong, G. P. Barber, M. S. Cline, T. R. Dreszer, S. G. Heitner, D. Karolchik, W. J. Kent, V. M. Kirkup, L. R. Meyer, J. C. Long, M. Maddren, B. J. Raney, T. S. Furey, L. Song, L. L. Grasfeder, P. G. Giresi, B.-K. Lee, A. Battenhouse, N. C. Sheffield, J. M. Simon, K. A. Showers, A. Safi, D. London, A. A. Bhinge, C. Shestak, M. R. Schaner, S. Ki Kim, Z. Z. Zhang, P. A. Mieczkowski, J. O. Mieczkowska, Z. Liu, R. M. McDaniell, Y. Ni, N. U. Rashid, M. J. Kim, S. Adar, Z. Zhang, T. Wang, D. Winter, D. Keefe, E. Birney, V. R. Iyer, J. D. Lieb, G. E. Crawford, G. Li, K. S. Sandhu, M. Zheng, P. Wang, O. J. Luo, A. Shahab, M. J. Fullwood, X. Ruan, Y. Ruan, R. M. Myers, F. Pauli, B. A. Williams, J. Gertz, G. K. Marinov, T. E. Reddy, J. Vielmetter, E. Partridge, D. Trout, K. E. Varley, C. Gasper, A. Bansal, S. Pepke, P. Jain, H. Amrhein, K. M. Bowling, M. Anaya, M. K. Cross, B. King, M. A. Muratet, I. Antoshechkin, K. M. Newberry, K. McCue, A. S. Nesmith, K. I.

Fisher-Aylor, B. Pusey, G. DeSalvo, S. L. Parker, S. Balasubramanian, N. S. Davis, S. K. Meadows, T. Eggleston, C. Gunter, J. S. Newberry, S. E. Levy, D. M. Absher, A. Mortazavi, W. H. Wong, B. Wold, M. J. Blow, A. Visel, L. A. Pennachio, L. Elnitski, E. H. Margulies, S. C. J. Parker, H. M. Petrykowska, A. Abyzov, B. Aken, D. Barrell, G. Barson, A. Berry, A. Bignell, V. Boychenko, G. Bussotti, J. Chrast, C. Davidson, T. Derrien, G. Despacio-Reyes, M. Diekhans, I. Ezkurdia, A. Frankish, J. Gilbert, J. M. Gonzalez, E. Griffiths, R. Harte, D. A. Hendrix, C. Howald, T. Hunt, I. Jungreis, M. Kay, E. Khurana, F. Kokocinski, J. Leng, M. F. Lin, J. Loveland, Z. Lu, D. Manthravadi, M. Mariotti, J. Mudge, G. Mukherjee, C. Notredame, B. Pei, J. M. Rodriguez, G. Saunders, A. Sboner, S. Searle, C. Sisu, C. Snow, C. Steward, A. Tanzer, E. Tapanari, M. L. Tress, M. J. van Baren, N. Walters, S. Washietl, L. Wilming, A. Zadissa, Z. Zhang, M. Brent, D. Haussler, M. Kellis, A. Valencia, M. Gerstein, A. Reymond, R. Guigó, J. Harrow, T. J. Hubbard, S. G. Landt, S. Frietze, A. Abyzov, N. Addleman, R. P. Alexander, R. K. Auerbach, S. Balasubramanian, K. Bettinger, N. Bhardwaj, A. P. Boyle, A. R. Cao, P. Cayting, A. Charos, Y. Cheng, C. Cheng, C. Eastman, G. Euskirchen, J. D. Fleming, F. Grubert, L. Habegger, M. Hariharan, A. Harmanci, S. Iyengar, V. X. Jin, K. J. Karczewski, M. Kasowski, P. Lacroute, H. Lam, N. Lamarre-Vincent, J. Leng, J. Lian, M. Lindahl-Allen, R. Min, B. Miotto, H. Monahan, Z. Moqtaderi, X. J. Mu, H. O'Geen, Z. Ouyang, D. Patacsil, B. Pei, D. Raha, L. Ramirez, B. Reed, J. Rozowsky, A. Sboner, M. Shi, C. Sisu, T. Slifer, H. Witt, L. Wu, X. Xu, K.-K. Yan, X. Yang, K. Y. Yip, Z. Zhang, K. Struhl, S. M. Weissman, M. Gerstein, P. J. Farnham, M. Snyder, S. A. Tenenbaum, L. O. Penalva, F. Doyle, S. Karmakar, S. G. Landt, R. R. Bhanvadia, A. Choudhury, M. Domanus, L. Ma, J. Moran, D. Patacsil, T. Slifer, A. Victorsen, X. Yang, M. Snyder, K. P. White, T. Auer, L. Centanin, M. Eichenlaub, F. Gruhl, S. Heermann, B. Hoeckendorf, D. Inoue, T. Kellner, S. Kirchmaier, C. Mueller, R. Reinhardt, L. Schertel, S. Schneider, R. Sinn, B. Wittbrodt, J. Wittbrodt, Z. Weng, T. W. Whitfield, J. Wang, P. J. Collins, S. F. Aldred, N. D. Trinklein, E. C. Partridge, R. M. Myers, J. Dekker, G. Jain, B. R. Lajoie, A. Sanyal, G. Balasundaram, D. L. Bates, R. Byron, T. K. Canfield, M. J. Diegel, D. Dunn, A. K. Ebersol, T. Frum, K. Garg, E. Gist, R. S. Hansen, L. Boatman, E. Haugen, R. Humbert, G. Jain, A. K. Johnson, E. M.

Johnson, T. V. Kutyavin, B. R. Lajoie, K. Lee, D. Lotakis, M. T. Maurano, S. J. Neph, F. V. Neri, E. D. Nguyen, H. Qu, A. P. Reynolds, V. Roach, E. Rynes, P. Sabo, M. E. Sanchez, R. S. Sandstrom, A. Sanyal, A. O. Shafer, A. B. Stergachis, S. Thomas, R. E. Thurman, B. Vernot, J. Vierstra, S. Vong, H. Wang, M. A. Weaver, Y. Yan, M. Zhang, J. M. Akey, M. Bender, M. O. Dorschner, M. Groudine, M. J. MacCoss, P. Navas, G. Stamatoyannopoulos, R. Kaul, J. Dekker, J. A. Stamatoyannopoulos, I. Dunham, K. Beal, A. Brazma, P. Flicek, J. Herrero, N. Johnson, D. Keefe, M. Lukk, N. M. Luscombe, D. Sobral, J. M. Vaquerizas, S. P. Wilder, S. Batzoglou, A. Sidow, N. Hussami, S. Kyriazopoulou-Panagiotopoulou, M. W. Libbrecht, M. A. Schaub, A. Kundaje, R. C. Hardison, W. Miller, B. Giardine, R. S. Harris, W. Wu, P. J. Bickel, B. Banfai, N. P. Boley, J. B. Brown, H. Huang, Q. Li, J. J. Li, W. S. Noble, J. A. Bilmes, O. J. Buske, M. M. Hoffman, A. D. Sahu, P. V. Kharchenko, P. J. Park, D. Baker, J. Taylor, Z. Weng, S. Iyer, X. Dong, M. Greven, X. Lin, J. Wang, H. S. Xi, J. Zhuang, M. Gerstein, R. P. Alexander, S. Balasubramanian, C. Cheng, A. Harmanci, L. Lochovsky, R. Min, X. J. Mu, J. Rozowsky, K.-K. Yan, K. Y. Yip and E. Birney, "An Integrated Encyclopedia of DNA Elements in the Human Genome", *Nature*, Vol. 489, No. 7414, pp. 57–74, 2012.

41. Untergasser, A., I. Cutcutache, T. Koressaar, J. Ye, B. C. Faircloth, M. Remm and S. G. Rozen, "Primer3–New Capabilities and Interfaces.", *Nucleic Acids Research*, Vol. 40, No. 15, p. e115, 2012.

42. Yang, H., H. Wang and R. Jaenisch, "Generating Genetically Modified Mice Using CRISPR/Cas-mediated Genome Engineering", *Nature Protocols*, Vol. 9, No. 8, pp. 1956–1968, 2014.

43. Zerbino, D. R., P. Achuthan, W. Akanni, M. R. Amode, D. Barrell, J. Bhai, K. Billis, C. Cummins, A. Gall, C. G. Girón, L. Gil, L. Gordon, L. Haggerty, E. Haskell, T. Hourlier, O. G. Izuogu, S. H. Janacek, T. Juettemann, J. K. To, M. R. Laird, I. Lavidas, Z. Liu, J. E. Loveland, T. Maurel, W. McLaren, B. Moore, J. Mudge, D. N. Murphy, V. Newman, M. Nuhn, D. Ogeh, C. K. Ong, A. Parker, M. Patri-

cio, H. S. Riat, H. Schuilenburg, D. Sheppard, H. Sparrow, K. Taylor, A. Thormann, A. Vullo, B. Walts, A. Zadissa, A. Frankish, S. E. Hunt, M. Kostadima, N. Langridge, F. J. Martin, M. Muffato, E. Perry, M. Ruffier, D. M. Staines, S. J. Trevanion, B. L. Aken, F. Cunningham, A. Yates and P. Flicek, "Ensembl 2018", *Nucleic Acids Research*, Vol. 46, No. D1, pp. D754–D761, 2018.

44. Concordet, J.-P. and M. Haeussler, "CRISPOR: Intuitive Guide Selection for CRISPR/Cas9 Genome Editing Experiments and Screens", *Nucleic Acids Research*, Vol. 46, No. W1, pp. W242–W245, 2018.

45. Hung, S. S., V. Chrysostomou, F. Li, J. K. Lim, J. H. Wang, J. E. Powell, L. Tu, M. Daniszewski, C. Lo, R. C. Wong, J. G. Crowston, A. Pébay, A. E. King, B. V. Bui, G. S. Liu and A. W. Hewitt, "AAV-Mediated CRISPR/Cas Gene Editing of Retinal Cells in Vivo", *Investigative Ophthalmology and Visual Science*, Vol. 57, No. 7, pp. 3470–3476, 2016.

46. Kaspar, B. K., B. Vissel, T. Bengoechea, S. Crone, L. Randolph-Moore, R. Muller, E. P. Brandon, D. Schaffer, I. M. Verma and K.-F. Lee, "Adeno-Associated Virus Effectively Mediates Conditional Gene Modification in the Brain", *Proceedings of the National Academy of Sciences*, Vol. 99, No. 4, pp. 2320–2325, 2002.

47. Thornton, B. and C. Basu, "Real-Time PCR (qPCR) Primer Design Using Free Online Software", *Biochemistry and Molecular Biology Education*, Vol. 39, No. 2, pp. 145–154, 2011.

48. Lein, E. S., M. J. Hawrylycz, N. Ao, M. Ayres, A. Bensinger, A. Bernard, A. F. Boe, M. S. Boguski, K. S. Brockway and E. J. Byrnes, "Genome-Wide Atlas of Gene Expression in the Adult Mouse Brain", *Nature*, Vol. 445, No. 7124, pp. 168–176, 2007.

49. Vanti, W. B., T. Nguyen, R. Cheng, K. R. Lynch, S. R. George and B. F. O'Dowd, "Novel Human G-Protein-Coupled Receptors", *Biochemical and Biophysical Research Communications*, Vol. 305, No. 1, pp. 67–71, 2003.

50. Shehata, M. A., A. C. Nøhr, D. Lissa, C. Bisig, V. Isberg, K. B. Andersen, K. Harpsøe, F. Björkling, H. Bräuner-Osborne and D. E. Gloriam, "Novel Agonist Bioisosteres and Common Structure-Activity Relationships for the Orphan G Protein-Coupled Receptor GPR139", *Scientific Reports*, Vol. 6, No. 1, pp. 1–13, 2016.

51. Nøhr, A. C., W. Jespers, M. A. Shehata, L. Floryan, V. Isberg, K. B. Andersen, J. Åqvist, H. Gutiérrez-de Terán, H. Bräuner-Osborne and D. E. Gloriam, "The GPR139 Reference Agonists 1a and 7c, and Tryptophan and Phenylalanine Share a Common Binding Site", *Scientific Reports*, Vol. 7, No. 1, pp. 1–9, 2017.

52. Nøhr, A. C., M. A. Shehata, A. S. Hauser, V. Isberg, J. Mokrosinski, K. B. Andersen, I. S. Farooqi, D. S. Pedersen, D. E. Gloriam and H. Bräuner-Osborne, "The Orphan G Protein-Coupled Receptor GPR139 is Activated by the Peptides: Adrenocorticotropic Hormone (ACTH), α-, and β-Melanocyte Stimulating Hormone (α-MSH, and β-MSH), and the Conserved Core Motif HFRW", *Neurochemistry International*, Vol. 102, pp. 105–113, 2017.

53. Consortium, E. P., "An Integrated encyclopedia of DNA Elements in the Human Genome", *Nature*, Vol. 489, No. 7414, p. 57, 2012.

54. He, P., B. A. Williams, D. Trout, G. K. Marinov, H. Amrhein, L. Berghella, S.-T. Goh, I. Plajzer-Frick, V. Afzal and L. A. Pennacchio, "The Changing Mouse Embryo Transcriptome at Whole Tissue and Single-Cell Resolution", *Nature*, Vol. 583, No. 7818, pp. 760–767, 2020.

55. Moore, L. D., T. Le and G. Fan, "DNA Methylation and Its Basic Function", *Neuropsychopharmacology*, Vol. 38, No. 1, pp. 23–38, 2013.

56. Gates, L. A., J. Shi, A. D. Rohira, Q. Feng, B. Zhu, M. T. Bedford, C. A. Sagum, S. Y. Jung, J. Qin and M.-J. Tsai, "Acetylation on Histone H3 Lysine 9 Mediates a Switch from Transcription Initiation to Elongation", *Journal of Biological Chemistry*, Vol. 292, No. 35, pp. 14456–14472, 2017.

57. Barski, A., S. Cuddapah, K. Cui, T.-Y. Roh, D. E. Schones, Z. Wang, G. Wei, I. Chepelev and K. Zhao, "High-Resolution Profiling of Histone Methylations in the Human Genome", *Cell*, Vol. 129, No. 4, pp. 823–837, 2007.

58. Bernstein, B. E., T. S. Mikkelsen, X. Xie, M. Kamal, D. J. Huebert, J. Cuff, B. Fry, A. Meissner, M. Wernig and K. Plath, "A Bivalent Chromatin Structure Marks Key Developmental Genes in Embryonic Stem Cells", *Cell*, Vol. 125, No. 2, pp. 315–326, 2006.

59. Dandan, W., S. H. M, Z. Stefano, D. Maria, O. Cesare, S. Chenghui, M. Ikuo, J. Caitlin, O. K. J, G. A. C, G. M. S, L. E. A, G. Brock and M. K. A, "Genetic Behavioral Screen Identifies an Orphan Anti-Opioid System", *Science*, Vol. 365, No. 6459, pp. 1267–1273, 2019.

60. Peng, J., "Gene Redundancy and Gene Compensation: An Updated View", *Journal of Genetics and Genomics*, Vol. 46, No. 7, pp. 329–333, 2019.

61. Buglo, E., E. Sarmiento, N. B. Martuscelli, D. W. Sant, M. C. Danzi, A. J. Abrams, J. E. Dallman and S. Züchner, "Genetic Compensation in a Stable Slc25a46 Mutant Zebrafish: A Case for Using F0 CRISPR Mutagenesis to Study Phenotypes Caused by Inherited Disease", *PloS One*, Vol. 15, No. 3, p. e0230566, 2020.

62. Rouf, M. A., L. Wen, Y. Mahendra, J. Wang, K. Zhang, S. Liang, Y. Wang, Z. Li, Y. Wang and G. Wang, "The Recent Advances and Future Perspectives of Genetic Compensation Studies in the Zebrafish Model", *Genes & Diseases*, 2022.

63. El-Brolosy, M. A. and D. Y. R. Stainier, "Genetic Compensation: A Phenomenon in Search of Mechanisms", *PLoS Genetics*, Vol. 13, No. 7, p. e1006780, 2017.

64. Platt, R., S. Chen, Y. Zhou, M. Yim, L. Swiech, H. Kempton, J. Dahlem, O. Parnas, T. Eisenhaure, M. Jovanovic, D. Graham, S. Jhunjhunwala, M. Heidenreich, R. Xavier, R. Langer, D. Anderson, N. Hacohen, A. Regev, G. Feng and F. Zhang, "CRISPR-Cas9 Knockin Mice for Genome Editing and Cancer Modeling", *Cell*,

Vol. 159, No. 2, pp. 440–455, 2014.